Improvement of sol models in Jorek with kinetic neutral particles coupled to MHD

Franssen, S.

Award date:
2018

IMPROVEMENT OF SOL MODELS IN JOREK WITH KINETIC NEUTRAL PARTICLES COUPLED TO MHD

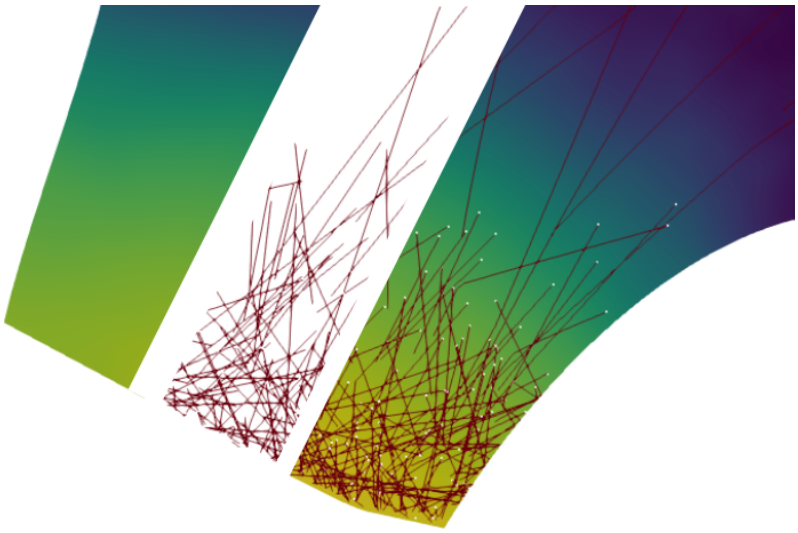

STIJN FRANSSEN

IMPROVEMENT OF SOL MODELS IN JOREK WITH KINETIC NEUTRAL PARTICLES COUPLED TO MHD

STIJN FRANSSEN BSc.

Supervision by: prof. dr. ir. Guido Huijsmans[*],
ir. Daan van Vugt[*,†] and dr. Alberto Loarte[†]

Master Science and Technology of Nuclear Fusion
Department of Applied Physics
[*]Eindhoven University of Technology
&
[†]ITER organisation

June 2018

ABSTRACT

Future nuclear fusion reactors will operate with a detached plasma, in order to simulate this the 3D non-linear magnetohydrodynamics code JOREK has been extended with kinetic neutral particles.

The physics of neutral particles has been added to the neutral particle extension of JOREK. This includes charge exchange and ionisation. For these neutral particles a gas puff source and a wall reflection source have been developed.

Feedback from JOREK to the particles has been implemented before, a coupling from the particle extension to JOREK was developed for this work. Allowing for simultaneous coupled runs of the code with its particle extension. An example run of a steady state plasma shows an increase of plasma density in the divertor.

SAMENVATTING

Toekomstige kernfusiereactoren zullen opereren met een plasma wat los staat van de wand. Om dit te simuleren is de 3D niet-lineaire magnetohydrodynamica code JOREK uitgebreid met kinetische neutrale deeltjes.

De fysica van ionisatie en *charge exchange*-ionisatie van neutrale deeltjes is toegevoegd aan de deeltjes uitbreiding van JOREK. Voor deze neutrale deeltjes zijn een gaspufbron en een wand-reflectiebron ontwikkeld.

Terugkoppeling van JOREK naar de deeltjes uitbreiding is al eerder gerealiseerd, voor dit werk is de terugkoppeling van de deeltjes code naar JOREK ontwikkeld. Hierdoor is het mogelijk om gekoppelde simulaties van JOREK en de deeltjes code uit te voeren. Een voorbeeld simulatie van een stabiel plasma laat een toename van de plasma dichtheid in de *divertor* zien.

ACKNOWLEDGMENTS

I would like to thank my supervisors Alberto, Guido and especially Daan, for putting in the time and effort to help me create this work. I also got much needed help from the wonderful people at ITER, the JOREK team and everybody from the 5th floor.

I would like to thank my family, friends and fiancé for the moral support and pushing me to continue when I needed motivation, not only during my graduation but throughout my whole university life.

CONTENTS

LIST OF FIGURES

LIST OF TABLES

LISTINGS

LIST OF ABRREVIATIONS

CO_2	carbon dioxide
IPCC	Intergovernmental Panel on Climate Change
SOL	Scrape Off Layer
ELM	Edge Localised Modes
MHD	magnetohydrodynamics

1 INTRODUCTION

Most energy needs of the modern world, such as energy for heating, housing, transportation and the production of food, are met or supported by fossil fuels like oil, coal, and natural gas. However the usage of these fuels has led to a sharp increase in the amount of carbon dioxide (CO_2) in the global atmosphere. As as consequence, the world average temperature in 2018 has increased by one degree Celsius (°C) when compared to pre-industrial levels [30]. If CO_2 emissions are not restrained the global temperature increase could be as large as $1.5\,°C$ by 2040, see figure 1.1. This will result in:

- A perturbing effect on climate, increasing risks of droughts and heavy precipitation;
- A rising sea level;
- melting of the polar ice caps;
- large detrimental effects on ecosystems;
- mass extinction of animal and plant species.

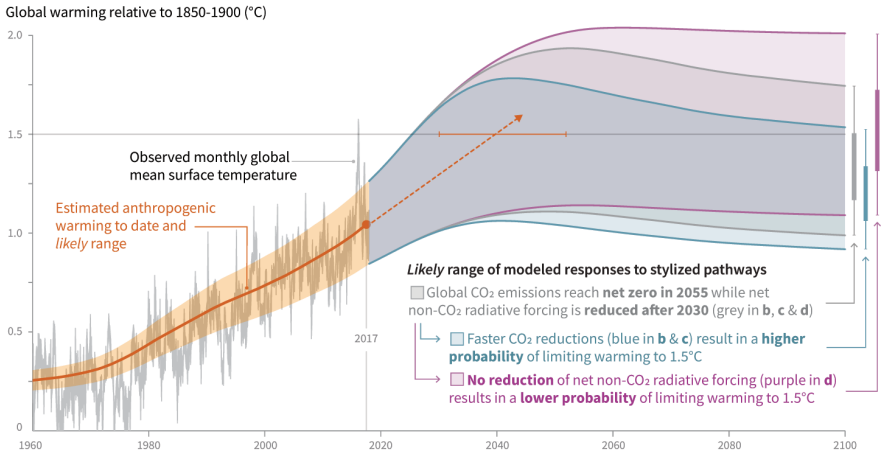

Figure 1.1: Historical data for global temperate change and modeled projection thereof based on anthropogenic CO_2 emissions. Image adapted from [30].

1.1 ALTERNATIVES TO FOSSIL FUELS

In order to mitigate the detrimental effects of anthropogenic global warming, the Intergovernmental Panel on Climate Change (IPCC)

warns that this temperature increase should be limited to no more then $1.5\,^{\circ}\mathrm{C}$. In order to achieve this the global energy infrastructure needs to wean from fossil fuels and transition to CO_2 neutral sources, such as photovoltaic solar energy and wind energy. However these sources don't come without difficulties.

1.1.1 *Limitations to conventional renewable sources*

A big drawback of some current renewable sources is its availability or rather its unavailability. The most obvious example of solar power being unavailable is during the night when the panels produce no output, or their reduced efficiency when it is cloudy. This problem is further compounded with the fact that electricity usage is higher during winter [15], when days are shorter so there is less solar energy. In a similar fashion to solar power not always being available, wind power is also only intermittently available. Intermittency could be reduced by temporarily storing the energy in for example batteries, however the economical feasibility of such a construction is a question that still needs to be answered [40].

Another issue with these alternatives to fossil fuel is that they take up a large amount of space, which puts it in direct competition with space needed for housing and food production. An example of this is the Dutch solar park 'Zonnepark Budel' [39], built in 2018. This has a surface area of 0.6 square kilometer (km^2) a nominal peak power* of 43.8 megawatt (MW) and produces about 160 terajoule (TJ) per year. In comparison, the Magnum gas turbine at the Eemshaven has a surface area of $0.005\,\mathrm{km}^2$, and a nominal power which is almost 10 times larger $437\,\mathrm{MW}$. When assuming a capacity factor† of 55%, which is a reasonable estimation for that type of reactor [44, p. 177], the yearly output is about $7.6 \times 10^3\,\mathrm{TJ}$, which is almost 50 times larger than the output of Zonnepark Budel. Or, to summarize, to replace the Magnum gas turbine, a solar park of $30\,\mathrm{km}^2$ would be needed.

In 2016, the Netherlands used $4.3 \times 10^5\,\mathrm{TJ}$ of electricity [8]. If all that had to come from solar energy, a staggering $1636\,\mathrm{km}^2$ would have to be covered with solar panels, an area slightly larger than province of Utrecht. If one takes into account that all forms of energy have to come from renewables, not only the electricity, a total of $3.2 \times 10^6\,\mathrm{TJ}$ [9] has to be produced, which would mean that approximately $12\,500\,\mathrm{km}^2$ has to be covered, about 30% of the total area of the Netherlands.

---

* The nominal peak power for photovoltaic systems is obtained by testing (part of) the system under specified conditions like light intensity and ambient temperature. Because these conditions are generally not present the actual yearly output produced is a more insightful quantity.

† "The ratio of the net electricity generated, for the time considered, to the energy that could have been generated at continuous full-power operation during the same period." [46]

The high space usage feeds directly into the 'not in my backyard' sentimentality, which affects mostly the placement of large wind turbines on land (and recently also solar parks [35]) where citizens and local municipalities sue the national government [34] to stop the construction of windmills. Their construction on sea does not fare much better, with citizens claiming 'horizon pollution' [36] and fishermen fear for the future of their family businesses [17].

Most other renewable energy sources are not feasible in the Netherlands. For hydropower for example the height difference is not adequate to allow for energy harvesting, and for geothermal power there is not enough availability to make a meaningful contribution [26, 29].

1.1.2 *Nuclear fission*

Even though it is not plagued by the issues of unreliability and large space usage, energy from nuclear fission is also not well loved, albeit for a different reason.

Nuclear fission is the process where heavy atomic nuclei split into two or more lighter products. The combined mass of the remaining products is slightly lower then the initial nucleus, and by the famous equation of Albert Einstein:

$$E = mc^2, \tag{1.1}$$

we know that the lost mass (m) will be transformed into an amount of energy (E), proportional to the square of the speed of light (c) [14, p. 23].

Humankind learned how to harness this process using nuclear reactors, but the catastrophes of Chernobyl in 1986 and Fukushima in 2011 made the technology unpopular with the public. The latter of the two, for example, was a major factor in the phasing out of nuclear energy in the Germany in their *Energiewende* (energy transition) [1].

Although modern reactors do not pose the same safety risks as the older reactors [50], an other unsolved problem with nuclear fission is what to do with the highly radio active long-lived waste it produces. This long-lived waste can have a half life between 24000 and up to 1 million years [42, 45]. Although used fuel can be reprocessed, this is a costly endeavour which still leaves the material active for 9000 years [51]. As of now there is no other way to manage this waste, other than storing it underground.

1.2 NUCLEAR FUSION

The inverse process of nuclear fission is the process of nuclear fusion: two nuclei fuse together. If the product of this process is lighter than

the initial components combined, energy is gained, as described by equation 1.1.

1.2.1 *Fuel of the stars*

Nuclear fusion is the primordial energy source of the universe, it is the process that powers stars. For example, in our sun, under the immense pressure generated by its gravitational force, hydrogen nuclei get converted to helium by a fusion process. The energy that is generated by these reactions is transmitted in the form of light and is the energy source for almost all life on earth [11].

1.2.2 *Fusion reaction*

The nuclei in a fusion reaction are positively charged, thus they repel each other. Only when they come close enough together the strong nuclear force between the subatomic particles will take over and fusion will occur. In the sun the gravitational force helps to overcome this barrier, however on earth there is not enough mass to confine the particles by gravitation.

Instead of relying on gravity to bring the particles close together, they can be made to collide with a large enough velocity in order to overcome the barrier. The velocity of particles on a micro scale can be compared to temperature on a macro scale [37], this means that the fusion fuel must be heated to extreme temperatures.

A measure of how often a fusion reaction occurs is the *reaction rate*. A higher reaction rate (more fusion reaction per time) at a lower temperature (lower so it is more readily achieved) is desirable. From figure 1.2 it can be seen that the reaction with these desired characteristics is the fusion of two specific isotopes of hydrogen [14]:

- Deuterium (D), containing a proton and *one* neutron;
- Tritium (T), containing a proton and *two* neutrons.

The fusion reaction between these two elements, results in a helium nucleus and a neutron, as depicted in figure 1.3 and shown in the following equation:

$$\mathrm{D} + \mathrm{T} \longrightarrow {}^{4}\mathrm{He} + \mathrm{n} + 17.58\,\mathrm{MeV}\,. \tag{1.2}$$

The 17.58 mega electronvolt* (MeV) gained in this process is divided over the neutron and helium ion in the form of kinetic energy, where the neutron end up with $14.1\,\mathrm{MeV}$ and the ion with $3.5\,\mathrm{MeV}$.

* In fusion the energies of single particles are often described using the electronvolt (eV), which is a more intuitive measure of its energy. An eV is defined as: the energy an electron gains when moving across a potential difference of 1 volt. Thus giving it the energy of 1 volt times the elementary charge: $1\,\mathrm{eV} \approx 1.6 \times 10^{-19}\,\mathrm{J}$.

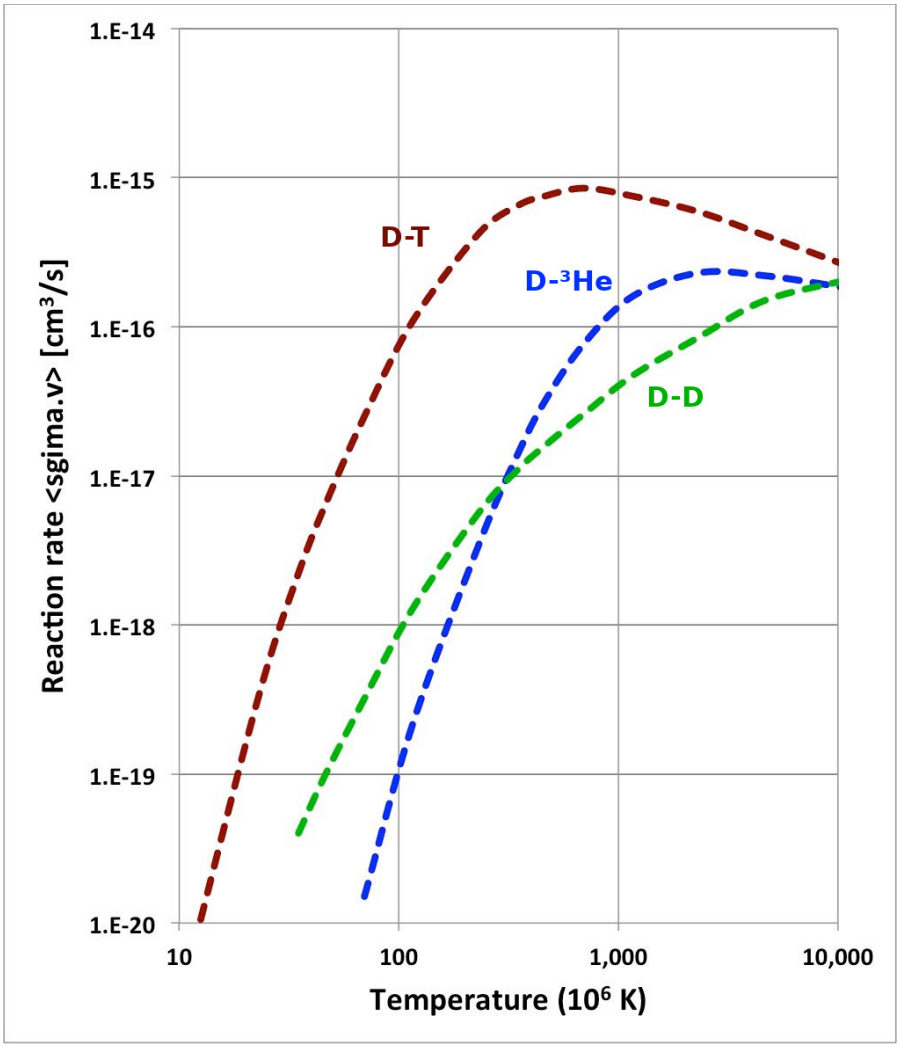

Figure 1.2: Reaction rates for the most relevant fusion reactions: deuterium-tritium, deuterium-helium-3 and deuterium-deuterium fusion. Image adapted from [6].

The mass of one D-T pair is approximately equal to 5 atomic mass units (u), which is approximately equal to $8.3 \times 10^{-27}\,\mathrm{kg}$, and will yield the aforementioned $17.58\,\mathrm{MeV}$, so $1\,\mathrm{kg}$ will yield $339\,\mathrm{TJ}$. To satisfy the total yearly energy usage of the Netherlands, assuming perfect conversion, only about $1300\,\mathrm{kg}$ of fuel would be needed. To put this into perspective, the energy released with the combustion of $1\,\mathrm{kg}$ of methane yields only $55.5\,\mathrm{MJ}$. To power the Netherlands with power plants such as the Magnum, mentioned in section 1.1.1, $7.7 \times 10^{9}\,\mathrm{kg}$ of methane would be needed yearly.

1.2.3 *Tokamak*

The most promising path to realising fusion uses the concept of a tokamak. It is a doughnut shaped (toroidal) device which uses strong

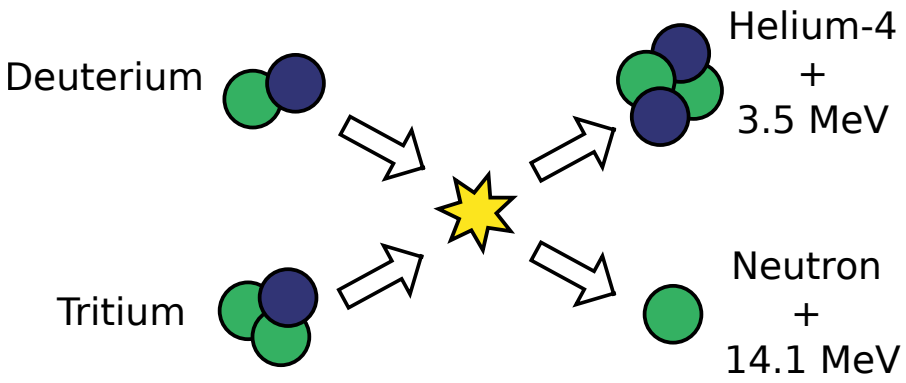

Figure 1.3: Schematic depiction of deuterium-tritium fusion, with as result helium and a neutron. Neutrons are depicted green and protons are coloured blue. Image adapted from [31].

magnetic fields to contain a high temperature plasma of deuterium and tritium, as shown in figure 1.4*.

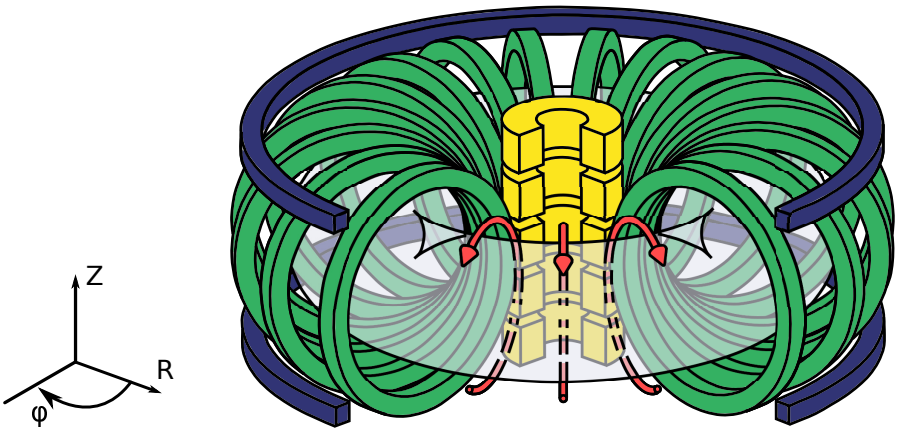

Figure 1.4: Schematic depiction of a tokamak. Shown are in yellow the central solenoid, green the toroidal field coils, and in blue the vertical field coils. The transparent white area is the plasma. The plasma has a toroidal shape, the $\hat{\varphi}$ direction is the toroidal direction, the red arrows indicate the poloidal direction. The axis for the cylindrical coordinates used are shown left. The major radius of the device is the distance from the center of the tokamak to the center of the poloidal cross-section. Image adapted from [32].

In the tokamak the fuel is heated to extreme temperatures of about 150 million kelvin (K) in order to facilitate the fusion reaction. No solid material can contain particles at such a temperature and survive. However at these temperatures most matter is in the state of a plasma, where most positively charged atom nuclei have lost their accompanying negatively charged electrons. Because the particles in a plasma are charged they can be influenced by electro-magnetic forces. The toroidal field coils of a tokamak, together with the current in the

* Normalized basis vectors are denoted with a hat, e. g. $\hat{\varphi}$ for the toroidal direction.

plasma that is induced by the central solenoid, create a magnetic cage that hold the hot plasma. The magnetic field lines resulting from the toroidal field coils and the plasma current have a helical shape and go around the vessel.

A charged particle gyrates around the field lines due to the Lorentz force, thus it follows them. This results in low particle and energy transport perpendicular to the field lines (in the poloidal direction), but virtually unimpeded transport along the field lines (in the toroidal direction).

In figure 1.4 the plasma was shown to have a circular cross-section, modern devices have extra coils that are used to shape the plasma into an elliptical shape (to increase the volume and improve the stability properties), figures 1.5 shows an example of the cross-section (i. e. a slice of the vessel in the RZ-plane) of such a device. Magnetic field lines that close upon themselves without going through solid material keep the bulk of the plasma confined in tokamak, this plasma makes up the core plasma. However at some point there will be field lines that will have to pass through parts of the reactor, these 'open field lines' are made to terminate on the divertor region. The thin layer of plasma that follows these field lines constitutes the region known as the Scrape Off Layer (SOL), it carries the hot particles escaping the core plasma to the divertor.

The confinement of particles is not perfect and particles continuously leave via the SOL. More problematic is when, due to perturbations to the plasma or instabilities in the plasma, a large amount of particles escape in a short amount of time (a few milliseconds), such events are called Edge Localised Modes (ELM). The escaping particles have energies large enough to displace the atoms making up the lattice of the divertor when they bombard it, a process called physical sputtering. The displaced atoms either get redeposited on the divertor or enter and pollute the plasma. Together with the fact that the high heat flux can melt parts of the divertor, ELMs can cause significantly enhanced erosion of the plasma vessel, thus reducing its lifetime [6].

When in the future these and other difficulties have been overcome, a power plant based on a tokamak could have some of the desired qualities of a contemporary fossil fuel plant (i. e. low surface area usage and controllability), but at the same time it will have a small carbon foot print like renewable sources. Although the products of the deuterium-tritium reaction are not radioactive on their own, the highly energetic neutrons will irradiate the surrounding structure of the plasma vessel. However only a small amount of material will be affected. If the right materials are chosen their radioactivity levels will have decayed to acceptable levels after about 100 years [6].

Unfortunately the science and technology of nuclear fusion is not developed to the point where we can build power plants with a fusion reactor at its core. The first reactors are projected to be built

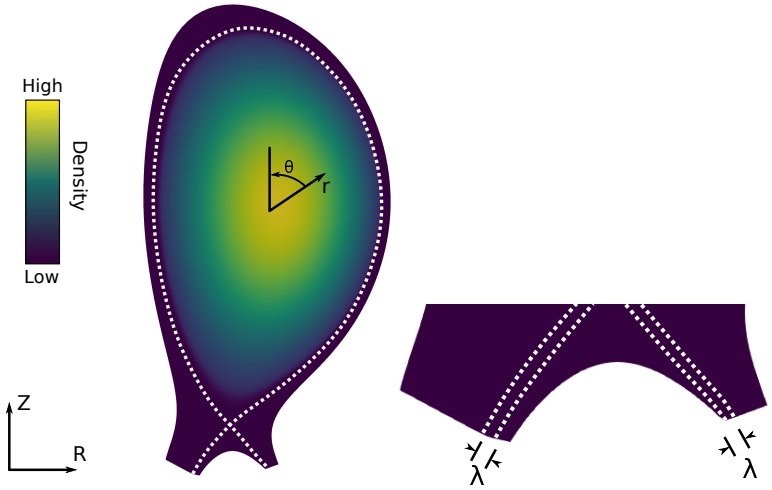

Figure 1.5: Schematic depiction of the particle density in the cross-section of the plasma in a tokamak (left). The axis left show the cylindrical coordinates. The axis inside the figure show the poloidal direction $\widehat{\theta}$ and the minor radius direction $\widehat{r}$. The white dashed line denotes the boundary just outside of the last closed flux surface, the SOL. Where the line crosses itself is called the X-point, here the poloidal magnetic field is zero. The line terminates on segments of the vessel called the divertor. The area between the X-point and the divertor is called the private region. Most of the particles are confined in the center, as is shown by the increasing density when moving in the negative $\widehat{r}$ direction.
On the right the private region is shown enlarged. The white dotted lines (not to scale) show the width of the SOL (λ).

in 2060, which is an optimistic estimate [28]. In order to build the first generation more knowledge needs to be gained by building and studying experimental reactors.

1.3 ITER

The largest tokamak experiment that is being developed at the moment is ITER, which is being built in the south of France, by the ITER members: China, the European Union, India, Japan, South-Korea, Russia and the United States. Its main goal is to produce a net energy gain. This energy gain is measured in the Q-factor:

$$Q = \frac{P_{\text{fusion}}}{P_{\text{heat}}}, \tag{1.3}$$

where P_{fusion} is the fusion power generated by the machine and P_{heat} is the power that is used to heat the fusion fuel. ITER will is projected to have $Q = 10$, and will be the first machine to have $Q > 1$.

The current record is $Q = 0.67$ which is held by the JET* tokamak. A major reason that ITER will surpass previous devices is because it is a larger device, from table 1.1 it can be seen that its R_{geo} is twice that of JET, resulting in an increase of almost a factor 30 in P_{fusion}. The heat will be better contained in ITER which can be seen from the energy confinement time (τ_E)[21], thus resulting a larger Q value.

1.3.1 *Scrape off layer*

One of the (many) challenges with building and operating a larger machine like ITER has to do with the SOL mentioned in section 1.2.3. The width of the SOL, depicted in figure 1.5, scales as reported by Eich et al. to be [13]:

$$L \propto B_{tor}^{-0.8} \cdot R_{geo}^{0} \cdot P_{SOL}^{0.1} \cdot q_{95}^{1.1}, \tag{1.4}$$

where B_{tor} is the toroidal component of the magnetic field, R_{geo} is the major radius of the device, P_{SOL} is the power flowing through the SOL and q_{95} is the safety factor† at the $95\,\%$ poloidal flux surface. Larger machines (i. e. machines with a larger major radius) will usually employ a similar or larger magnetic field, and thus will have a similar or smaller L. The foreseen SOL-width of ITER will be $L_I = 0.9\,\mathrm{mm}$ compared to that of JET $L_J = 1.2\,\mathrm{mm}$. The power that the ITER SOL will carry will be $100\,\mathrm{MW}$ while for JET it is only $12\,\mathrm{MW}$. So even though they have a similar size SOL, at ITER it will need to carry about a tenfold more power.

This power strikes the divertor, which can only handle the large particle and heat fluxes in steady state situations. There are multiple ways to decrease the heat load on the divertor, for example by magnetic perturbations to split the SOL [5]. For ITER the main strategy will be to operate with a detached divertor.

Table 1.1: Device parameters (expected values for ITER)[18]

Device	P_{fusion}	Energy content	R_{geo}	τ_E	Q	L
JET	16.7 MW	10 MJ	3 m	1 s	0.67	0.9 mm
ITER	500 MW	450 MJ	6.2 m	8 s	10	1.2 mm

* The Joined European Torus or JET is the largest European device, and holds the record for fusion power output of 16 MW. For more details see https://www.euro-fusion.org/devices/jet/.

† The safety factor is a measure of the helicity of the magnetic field. When following a field line, q is the amount of toroidal turns are needed before a poloidal turn has been made.

1.3.2 *Need for a detached divertor*

Detached divertor tokamak operation can be achieved by having a high neutral and impurity gas density, like neon, in the divertor region [24, 25]. These neutrals and impurities will collide with the ions coming from the plasma taking part of their energy. This energy is then radiated away, thus reducing the power load on the divertor plates. Detached divertor operation is currently envisioned as 'the key element of the ITER baseline design' [24], and necessary for future tokamak designs as well.

1.4 SIMULATION

In order to prepare for ITER operation with a detached divertor, the plasma in the machine has to be simulated, so that favourable operating modes can be determined and problems can be identified. In principle this can be done by following each particle individually, calculating the forces that act on that particle (and the effect it will have on the other particles), and from there determine the trajectory of the particle. In ITER the peak density is in the order of $10^{20}\,\mathrm{m}^{-3}$ and the plasma volume is $800\,\mathrm{m}^3$, giving a total amount of particles of about 10^{21} [20]. At this point the fastest super computer in the world can do 144×10^{15} calculations per seconds [43]. Following all particles for only one time step, without (re)calculating the forces acting on the particles, will take about 2 hours. Incorporating feedback of all particles onto each other makes this endeavour not feasible. In order to still be able to simulate the tokamak a set of simplifications need to be made.

1.4.1 *Magnetohydrodynamics*

Water, when streaming from a faucet, is not experienced as a large amount of individual H_2O molecules, but rather as a continuous flow of a liquid. In the theory of fluids this characteristic is formalized by the *continuum assumption*, describing materials as a continuous mass instead of discrete particles. Gasses can often be characterised in a similar fashion, and the theory of fluids describe both gasses and liquids [33]. In order to describe plasmas, which are ionized gasses, the theory of magnetohydrodynamics (MHD) was developed by combining the theory of fluids and electrodynamics [14].

The validity of continuum assumption can be represented by the Knudsen number [33, p. 364]:

$$\mathrm{Kn} = \lambda / l. \tag{1.5}$$

Here λ is the mean free path of the particles and l is the typical length scale for the problem. When $\mathrm{Kn} > 1$ the continuum assumption breaks down, and the fluid description is no longer valid. For neutrals in the divertor λ is determined by the length the neutral can travel before a reaction process will alter its behaviour. In a divertor the SOL has wildly different parameters (like temperature and plasma density amongst others), thus its width is the typical length so $l \approx 1\,\mathrm{mm}$.

The mean free path for ionisation can be found as follows for a particle with velocity v:

$$\lambda_{\mathrm{ion}} = \frac{v}{R_{\mathrm{ion}} n_e}, \tag{1.6}$$

where R_{ion} is the ionisation rate and n_e is the electron density. Here the velocity of the particles is determined by assuming that the neutral particles will have an energy similar to the disassociation energy $E_{\mathrm{D,dis}} = 15.3\,\mathrm{eV}$ [27]. The velocity, of a particle with mass m is related to its energy via

$$E = \frac{1}{2} m v^2. \tag{1.7}$$

Combining equation 1.6 and 1.7 yields:

$$\lambda_{\mathrm{ion}} = \frac{1}{R_{\mathrm{ion}} n_e} \sqrt{\frac{2 E_{\mathrm{D,dis}}}{m}}, \tag{1.8}$$

and a similar equation can be found for the charge exchange mean free path length λ_{CX}. The quantity of interest is the effective mean free path:

$$\lambda_{\mathrm{eff}} = \left(\lambda_{\mathrm{ion}}^{-1} + \lambda_{\mathrm{CX}}^{-1}\right)^{-1} \tag{1.9}$$

The ionisation, recombination and charge exchange rates can be found using data from OPEN-ADAS [41] and are plotted using the atomic package for Python [38], see figure 1.6. From the recombination rates the mean free path and Knudsen numbers can be determined, see figure 1.7. As can be seen from the figure, the fluid approximation is not valid, thus particle behaviour has to be taken into account.

The mean free path for neutral-neutral collisions for a gas species n with density n_{n} and atom radius r_{n}, is given by [10, p. 88]:

$$\lambda_{\mathrm{nnc}} = \left(\sqrt{2} n_{\mathrm{n}} 4\pi r_{\mathrm{n}}^2\right)^{-1}. \tag{1.10}$$

In figure 1.8 the λ_{nnc} of hydrogen is plotted as a function of n_{n}. From this plot it can be seen that only for higher densities ($n_{\mathrm{n}} > 10^{21}\,\mathrm{m}^{-3}$), the mean free path will be comparable with the typical length within a divertor. This means that generally the neutral-neutral collisions can be ignored. However this does not hold for detached divertors, which can have a neutral density in that range [24].

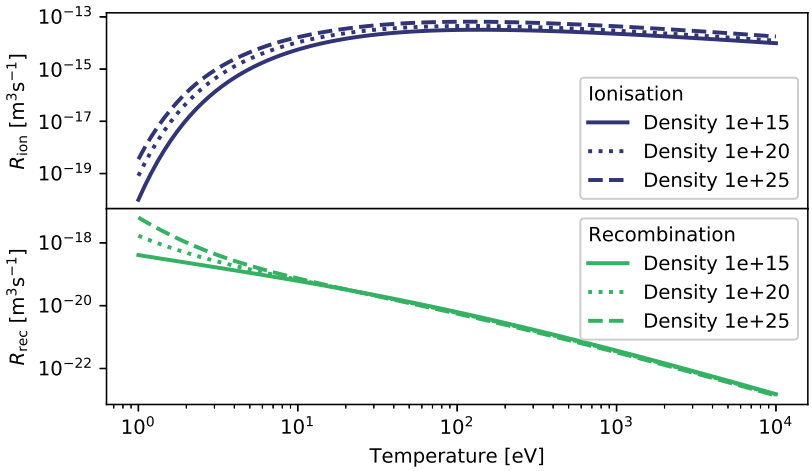

(a) Ionisation (blue) and recombination rates (green) in $\mathrm{m}^3\mathrm{s}^{-1}$ as a function of T_e for three different n_e.

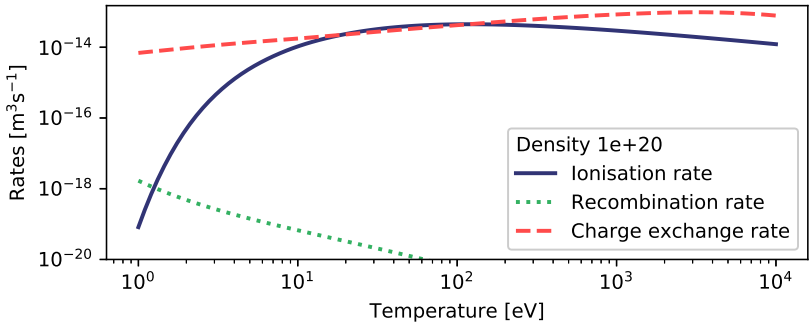

(b) Ionisation (blue), recombination (green) and charge exchange rates (red) as a function of T_e at $n_e = 1 \times 10^{20}\,\mathrm{m}^{-3}$

Figure 1.6: Ionisation, recombination and charge exchange rates for hydrogen as a function of T_e for different n_e. Data from the OPEN-ADAS project [41].

1.4.2 SOLPS

Because the continuum assumption breaks down for neutrals in the divertor their behaviour is not well described by the fluid theory. The go-to solution of the fusion community are hybrid solutions: hydrodynamic fluid models the plasma where appropriate, but at the edges model the neutrals with kinetic modeling. An example of such a package is SOLPS-ITER (SOLPS). It is a combination of the EIRENE and B2.5 codes [4, 49]. The first is a 3D kinetic Monte-Carlo neutral gas transport code, the later is a 2D multi-fluid plasma edge code.

The SOLPS code is mostly used for steady state heat fluxes in 2D axisymmetric equilibria. Moreover it assumes magnetic fields that are fixed in time, so it does not allow for simulations of MHD instabilities and their effects. Another limitation stems from the fact that EIRENE and B2.5 do not describe the core plasma, this means that behaviour

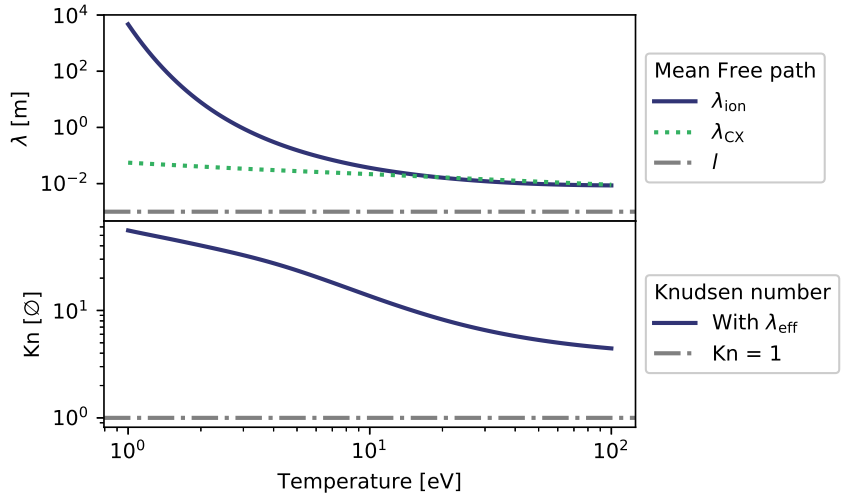

Figure 1.7: The top plot shows the mean free paths for ionisation and charge exchange as a function of T, for deuterium atoms with a kinetic energy of $E_{\mathrm{D,dis}} = 15.3\,\mathrm{eV}$ at $n_e = 10^{20}\,\mathrm{m}^{-3}$. The gray dash-dotted line shows the typical length in a divertor.
The bottom plot shows the Knudsen number with λ_{eff} as the mean free path as a function of T. The gray dash-dotted line indicates the turn over point $\mathrm{Kn} = 1$ the turning point for the validity of the continuum assumption.

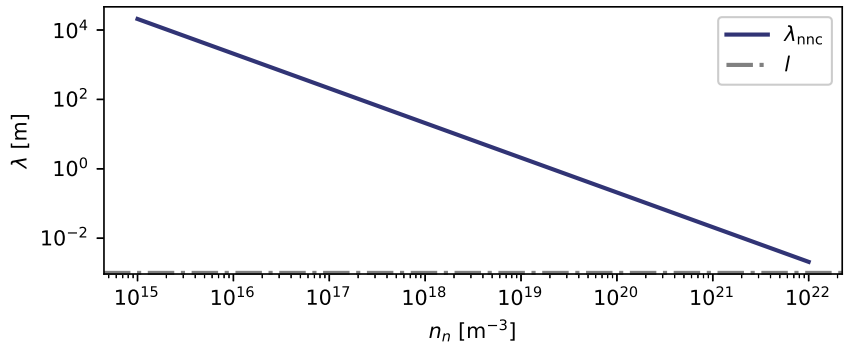

Figure 1.8: The mean free path for neutral-neutral collisions as a function of the neutral density is shown (in blue). The gray dash-dotted line is the typical length scale in a divertor.

are set as boundary conditions of these codes, thus increasing the number of free parameters in the system. These boundary conditions or profiles can be gotten from either comparing to experiments (which decreases predictive power), or by coupling the code to a core plasma code (further increasing the complexity of the overall system).

1.5 RESEARCH QUESTION

The stated limitations are avoided by using the JOREK code (which is a 3D MHD code which models the entire plasma) combined with its kinetic particle extension (see chapter 2), which will improve its divertor modeling. The focus of this thesis is adding neutral particle support for the particle extension of JOREK. Also the effect of these neutrals should be coupled to main MHD code of JOREK. The work is guided by the following design assignment:

> Improving the particle code extension of JOREK by adding neutral particles and their behaviour and coupling feedback of the particle extension to JOREK.

In the following chapters the improvement of the JOREK particle extension is described, after the workings of both JOREK and the particle code as they were before the improvement.

In chapters 3 and 4 the physics of neutral particles will be described, where the different behaviours of the neutrals and the sources and sinks the implemented sources and sinks.

In chapter 5 the coupling and feedback of the particle code to JOREK that has been implemented will be described. After which an example coupled run of the neutral particles is shown.

Finally in chapter 6 the current state and recommendations for further development are given.

2

SIMULATING PLASMAS AND PARTICLES WITH JOREK

Before the additions to the existing models can be explained, more background information needs to be given. In this chapter first the JOREK code will be discussed and subsequently its particle extension will be examined.

2.1 JOREK

In order to simulate the behaviour of MHD instabilities in a plasma in a tokamak, JOREK solves the MHD equations [19]. Space is discretized in two different ways:

- In the poloidal plane bicubic finite elements (i. e. 2D final elements of the third order) describe the JOREK fields;
- In the toroidal direction the fields are described by a Fourier series.

The finite-elements have two element-local coordinates, which are called s and t. The variables and space can be described by the basis functions in the elements, thus the elements can be curved in RZ (i. e. real) space. The distribution of a quantity $X(s,t)$ within a certain element is given by:

$$X(s,t) = \sum_{k=1}^{4} \sum_{l=1}^{4} X_{k,l} P_{k,l}(s,t) \tag{2.1}$$

where $X_{k,l}$ are the expansion coefficients and $P_{k,l}$ are modified cubic Bernstein polynomials [47]. The discretization is described extensively in [12] and visualized in figure 2.1. Time stepping is done with a Crank–Nicolson scheme.

The version of JOREK that is being used is the so called 'model 303' which solves reduced MHD equations, in this thesis the three equations governing density, parallel momentum and energy of that model will be studied closely (see equations A.1 to A.3, in appendix A). Useful definitions and a list of variables used in the model can be found in tables A.1 and A.2 respectively. For a more extensive explanation of reduced MHD in jorek see [2].

The approach of solving the reduced MHD equations with the poloidal finite elements and toroidal Fourier series allows for 3D simulations of the core plasma, SOL and divertor region with a reasonable computational time.

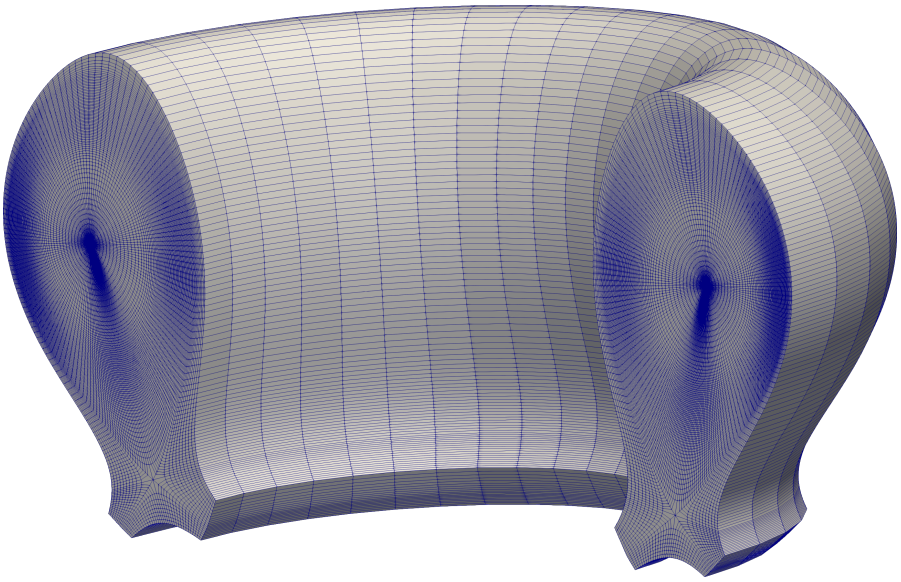

Figure 2.1: Depiction of discretization of space in JOREK. Although the toroidal discretization is shown using planes, in reality it is simulated using Fourier series. Reprinted with permission from [48].

Without the particle extension neutrals are not implemented in model 303.

2.2 PARTICLE EXTENSION

The kinetic particle tracer is a recent add-on of the JOREK code. A small overview of its functionality will be given, a more in depth explanation can be found in [48]. It uses a particle-in-cell method to track particles in real space. This means that one tracked unit represents a large amount of physical atoms. For the particles that are used in this thesis the information that is tracked can be found in table 2.1*.

Particle movement is simulated by using the Boris Scheme that solves the equation of motion for a single particle [3]:

$$\frac{\mathrm{d}\vec{v}}{\mathrm{d}t} = \frac{q}{m}\left[\vec{E} + \vec{v} \times \vec{B}\right]. \tag{2.2}$$

Since neutral particles have $q = 0$, the right hand side of the equation disappears. This means that the velocity of the particle remains unchanged from the initialisation, so it will fly straight in real space at a constant speed, but that path will be curved in the local finite element coordinates s and t.

An example workflow of running a simulation using the particle code starts with reading in previously simulated JOREK fields or equilibrium. After which a group of particles are created with the attributes

* The number between parenthesis after a variable denote the length of the vector it represents, e. g. `x(3)` has length 3 to store the R, Z, φ information.

Table 2.1: Particle variables

Variable	Description
`x(3)`	location in real space (i. e. in R, Z, φ space)
`st(2)`	location in element-local space (i. e. in s, t space)
`i_elm`	element number
`weight`	weight (the number of physical particles it represents)
`v(3)`	velocity
`q`	charge
`i_life`	number of times this particle has been initialized
`t_birth`	time stamp of last initialisation

Table 2.2: Particle group variables

Variable	Description
`Z`	Atomic number
`mass`	Mass of each particle
`ADF11_all`	OPEN-ADAS data files
`coronal`	equilibrium ionisation/recombination state information

described in table 2.2. Then the particles are initialized at a desired location and subsequently their other atributes found in table 2.1 are determined. The spatial distribution of the particles can be done uniformly over the domain or it can adhere to an arbitrary acceptance-rejection function (which can be made to depend on the JOREK fields). A set of events can be declared, these can be (amongst other things) reading in a different JOREK equilibrium, diagnostics such as counting all particles, or saving the state of all particles to a file. These events can be triggered at specific times or intervals.

Then the main particle loop is started. At the start of the loop the amount of particle steps that can be taken is calculated. For each particle the electric and magnetic fields at its location are determined, allowing the particle pusher to move the particle to its new location in real space (i. e. $RZ\varphi$-space). Then the new location in st-space and the JOREK element it is in are determined. Particle stepping is repeated until the next event time is reached. At that point the scheduled events are executed, and the main particle loop is repeated.

2.2.1 *Sputtering*

Since physical sputtering is an important effect if ELMs it has been implemented in the code as an event [23, 47]. When the event is run the flux of plasma particles to the wall is determined, and an appropriate amount of particles are added to the particle simulation to track. The

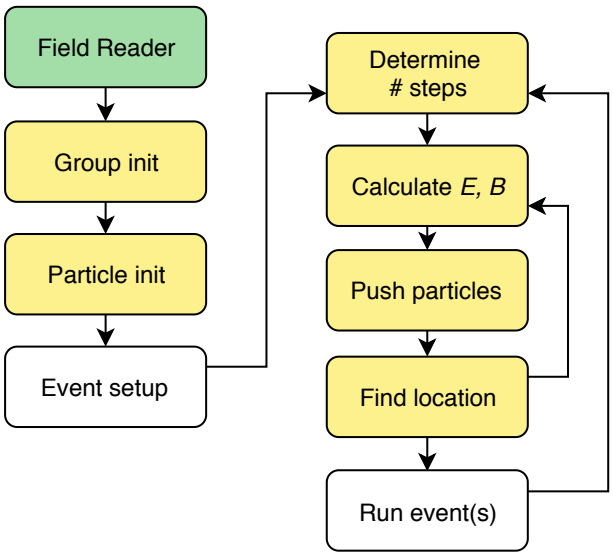

Figure 2.2: Example workflow for running a particle simulation. Green blocks indicate coupling between JOREK and the particle code. Yellow blocks indicate an action of the particle code. Event blocks are white.

amount of particles added and their initial energies are determined as a function of the incoming energy of the plasma flux and properties of the plasma facing components.

2.2.2 *Projection*

In order to include the contribution of the particle behaviour to the JOREK fields, that information, which is represented by point like particles in real space, needs to be projected onto the JOREK elements in st space. This in done in a projection event, which is one of the most relevant events for this thesis. The equation of the projection is given by [48]:

$$\int_V pv\, dV = \int_V \sum_i \delta(\vec{x} - \vec{x}_i)\, X w_i v\, dV, \tag{2.3}$$

Where p is the projected quantity in weak form, X is the moment to be projected (e. g. 1 for number density, m for mass density, $p_{\|}$ for parallel momentum, E for energy et cetera), w_i is the weight of particle i, and v is a basis function. Since particles are modeled as points in space, they are represented using Dirac delta functions $\delta(\vec{x})$, where $\vec{x}$ is the location in RZ-space.

The point-like representation of the particles in real space can lead to problems when projecting on the finite element description, therefore

a smoothing factor λ and hyper smoothing factor ζ are added. The projection equation then becomes:

$$\int \left[pv + \lambda \nabla p \cdot \nabla v + \zeta \nabla^2 p \nabla^2 v\right] \, dV = \int \sum_i \delta(\vec{x} - \vec{x}_i) w_i v \, dV, \quad (2.4)$$

with ∇^2 the Laplacian operator. An example of the density projection, with and without smoothing, is given in figure 2.3. From this figure it can be clearly seen that without any smoothing the projection has artifacts spreading away from the particle distribution (figure 2.3b). By only applying regular smoothing the artifacts mostly disappear. By also adding hyper smoothing the projection becomes slightly more defined in space. With the use of the (hyper) smoothing factors the particle distribution becomes less sharply defined in space, but it should be noted that the particle distribution is highly artificial and in real simulations the effects will be less profound.

The need for smoothing can be avoided if a large enough number of particles is simulated. However this also increases computational load, therefore a balance has to be made.

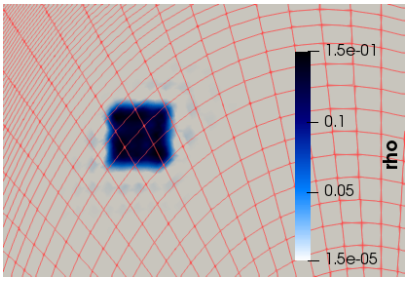

(a) Linear scale, $\lambda = 0$ and $\zeta = 0$.

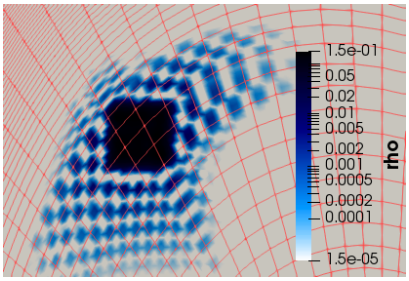

(b) Logarithmic scale, $\lambda = 0$ and $\zeta = 0$.

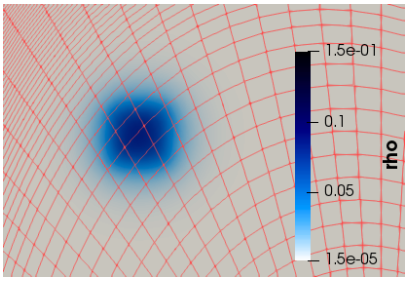

(c) Linear scale, $\lambda = 1 \times 10^{-3}$ and $\zeta = 0$.

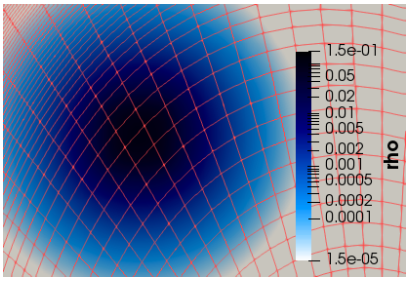

(d) Logarithmic scale, $\lambda = 1 \times 10^{-3}$ and $\zeta = 0$.

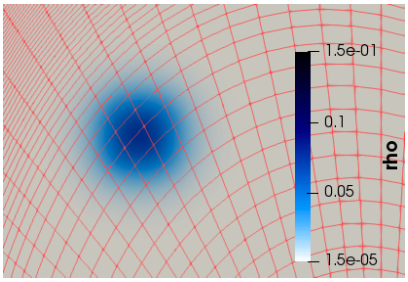

(e) Linear scale, $\lambda = 1 \times 10^{-3}$ and $\zeta = 1 \times 10^{-6}$.

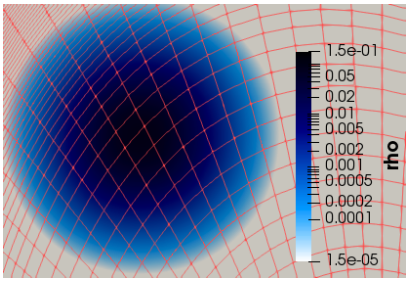

(f) Logarithmic scale, $\lambda = 1 \times 10^{-3}$ and $\zeta = 1 \times 10^{-6}$.

Figure 2.3: Projection of a set of 1×10^{19} particles are projected to jorek space for different smoothing parameters, the projected quantity is ρ. Overlaid is the JOREK grid.

3

NEUTRAL PARTICLES IN A TOKAMAK PLASMA

In this chapter the physics related to neutral particles in a tokamak plasma that has been implemented for this work will be described. This includes the ionisation of neutral particles and the charge exchange of neutrals with plasma particles. The particle workflow depicted in figure 2.2 is updated to include ionisation and charge exchange as depicted in figure 3.1.

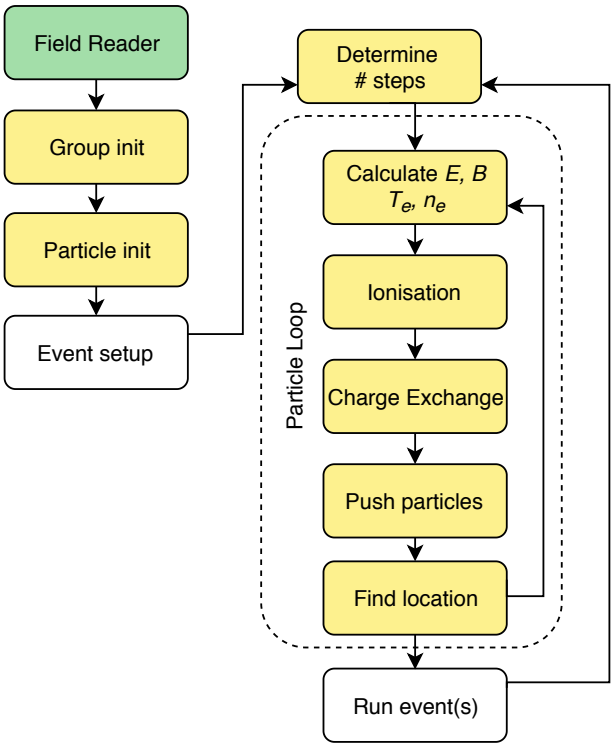

Figure 3.1: Updated workflow for a particle simulation, including a ionisation and charge exchange block.

3.1 IONISATION

Most particles in a tokamak plasma are ionized, and most neutrals will get to this state as well. The process of the ionisation of hydrogen, i. e. the process where neutral hydrogen loses its electron, is implemented in the code as follows. First different plasma quantities that influence the particle are determined at its location, these are the electron temperature T_e, the electron density n_e. With these the ionisation rate R_{ion}

is determined (in $\mathrm{m^3 s^{-1}}$) from the OPEN-ADAS data, then the ionisation probability is then calculated:

$$P_{\text{ion}} = 1 - \exp\left(-R_{\text{ion}} \cdot n_e \cdot \texttt{timesteps}\right), \tag{3.1}$$

where `timesteps` is the time step length for the particle code. If the `weight` of the particle, the physical number of atoms the particle represents, is lower then a set threshold value, the particle is thrown away if a random number $u_{R,1} \leq P_{\text{ion}}$. If the `weight` is above the threshold value, the weight is reduced (i. e. physical particles are removed from the simulations) by a factor $(1 - P_{\text{ion}})$. The described flow is shown in figure 3.2.

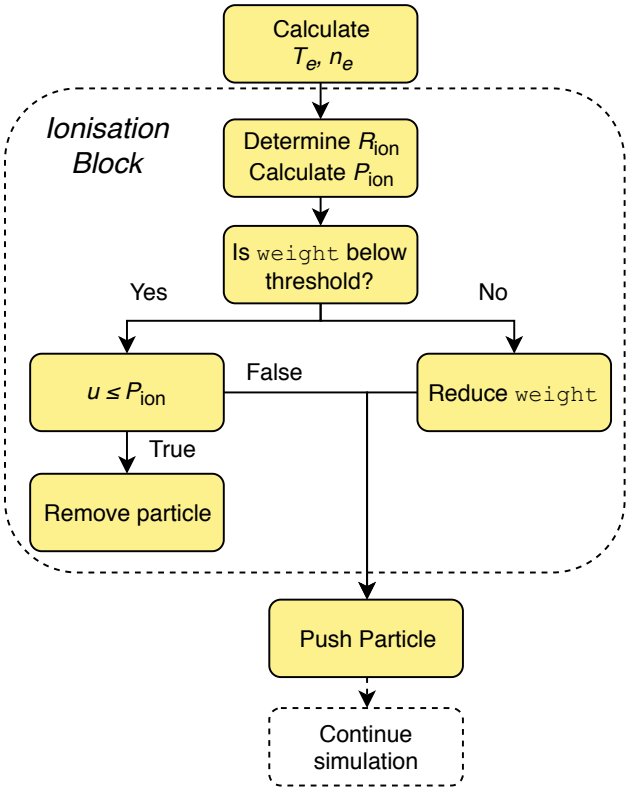

Figure 3.2: Workflow for ionisation.

3.2 CHARGE EXCHANGE

In a charge exchange event one particle will lose an electron to another particle. For hydrogen isotopes the reaction is*:

$$\mathrm{H^+ + H \longrightarrow H + H^+}\,. \tag{3.2}$$

So since a neutral particle will become a ion and vice versa, the total amount of ions and neutral particles will remain unchanged. This

* Negative (hydrogen) isotopes are not taken into consideration in this work.

process can be imagined as if a neutral particle gets a random velocity with a magnitude that corresponds to the local plasma parameters. It is implemented as follows: First, similar to how P_{ion} is calculated, the charge exchange rate R_{CX} is determined using T_e and n_e, from which the charge exchange probability is calculated using:

$$P_{\text{CX}} = 1 - \exp\left(-R_{\text{CX}} \cdot n_e \cdot \texttt{timesteps}\right). \tag{3.3}$$

Then this probability is compared to a random number $u_{R,2}$, if $u_{R,2} \leq P_{\text{CX}}$ a charge exchange will take place. To simplify implementation a fixed energy E_{sample} [J], is sampled and used to determine the new velocity as such [48]:

$$\texttt{v} = \sqrt{\frac{2E_{\text{sample}}}{\texttt{mass}}} \cdot \vec{u}_{R,3}, \tag{3.4}$$

where $\vec{u}_{R,3}$ is a vector with 3 random numbers. A more realistic approach would be sample velocities from a distorted Maxwellian distribution.

After the charge exchange event, the particle is pushed in space. At the moment the existing Boris pusher (as described in section section2.2) is used for this. The Boris pusher is designed to push electrically charged particles, and needs the electrical and magnetic field. Since the neutrals are not affected by these fields, it is possible to decrease the computational time needed if a simpler pusher would be implemented that does not take the fields into account.

The workflow of the charge exchange event can be seen in figure 3.4. An example of charge exchange events can been seen in figure 3.3.

3.3 RECOMBINATION

Recombination is the reverse process of ionisation: an ion and a electron combine to form an ion of with a higher charge, or a neutral atom. Due to time constraints recombination has not been implemented in this work.

The recombination source is similar to the ionisation source and given by:

$$S_{n,\text{re}} = R_{\text{re}}(n_e, T_e) n_e, \tag{3.5}$$

where R_{re} is the recombination rate rate, which is spline interpolated from OPEN-ADAS data depending on the local n_e and T_e.

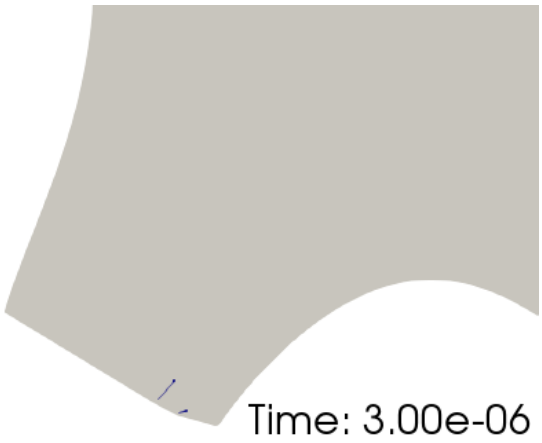

(a) At $t = 3\,\mu s$

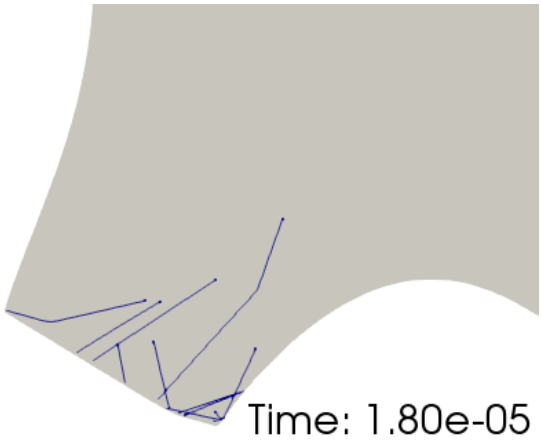

(b) At $t = 18\,\mu s$

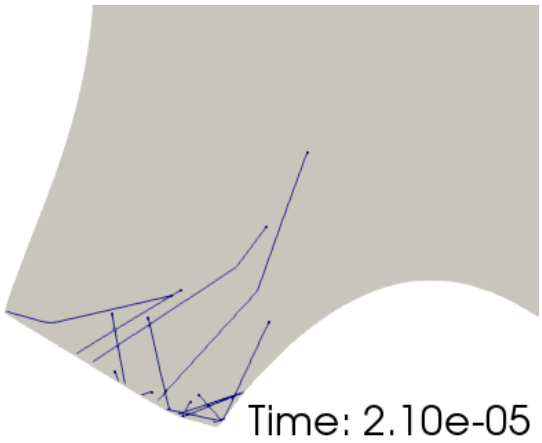

(c) At $t = 21\,\mu s$

Figure 3.3: Visualisation of charge exchange events. The neutrals fly straight until a charge event takes place, which alters their velocity, resulting in a sudden change of direction.

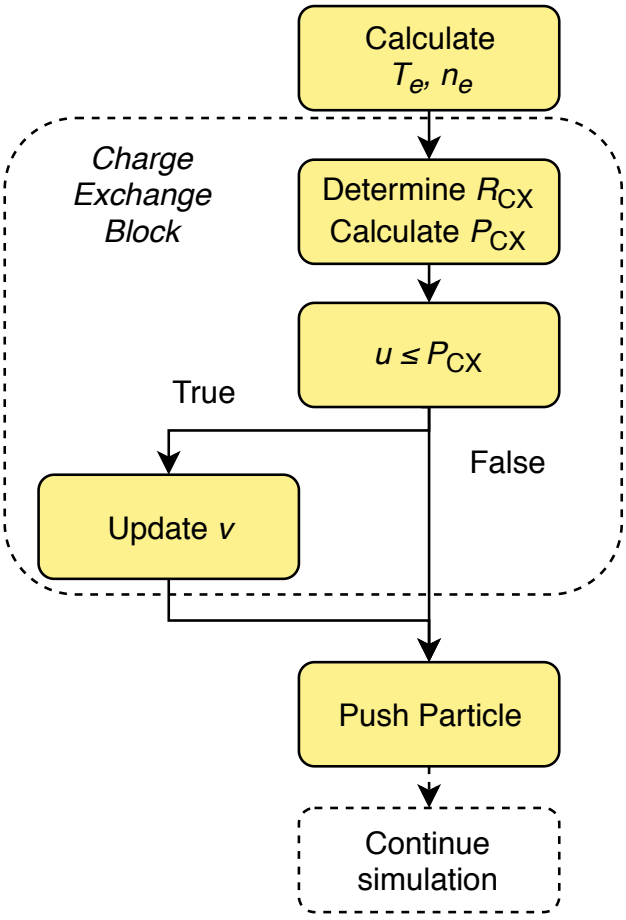

Figure 3.4: Workflow for charge exchange.

4 PARTICLE SOURCES AND SINKS

In a tokamak neutral particles are introduced by a variety of sources. The most important ones are gas introduced through valves, particles reflecting from the vessel walls, and the recombination of plasma ions into neutrals. In the previous chapter ionisation and recombination have been examined, so this chapter will focus on gas puffing and reflection. By modifying the reflection source a sink can be created.

4.1 GAS PUFFING

There are multiple reasons to add neutral particles to a tokamak plasma by means of gas valves, these include [22]:

- To fuel the plasma;
- To seed impurities in the divertor region;
- To increase the neutral pressure in the divertor region to allow for a detached divertor;
- To kill off the plasma by means of a massive gas injection.

This puffing, as it is called, has been implemented to be used in two different ways. If the `R`, `Z`, and `phi` (see table 4.1) location of the source are declared, it will function as a circular source with radius `valve_r` in the RZ-plane at the specified φ location, with its center at the specified R and Z location. If `phi` is omitted, it will behave as a toroidal source with minor radius `valve_r` at the specified R and Z location.

Table 4.1: Gas puffing variables.

Variable name	Description
`n_puff`	Number of super particles to puff $[\varnothing]$
`fueling_rate`	Fueling rate of the particles $[\mathrm{s}^{-1}]$
`R`, `Z`, `phi`*	Location of the particle source in real space $[\mathrm{m}]$
`valve_r`	Radius of the particle source $[\mathrm{m}]$
`rng`*	Random number generator to use
`seed`*	Seed for the random number generator

*optional variable

The source will initialize particles at random locations within the defined space, if `rng` is not specified it will default to a PCG32 random

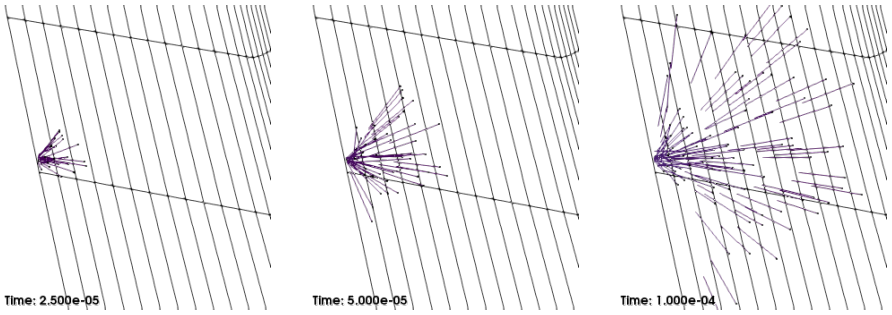

(a) At $t = 25\,\mu s$ (b) At $t = 50\,\mu s$ (c) At $t = 100\,\mu s$

Figure 4.1: A representation of the paths traveled by particles from puffing source at the edge of the vessel in the RZ-plane. Overlaid is the grid.

number generator. Gas that enters the vessel through a valve will consist of D_2 molecules. Since the dissociation process has not been modeled, it is assumed that the molecules will dissociate before tracing them with the particle code. So the neutral particles will have a velocity that corresponds to half of the dissociation energy of a D_2 atom: $2.28\,eV$ [27], thus resulting in a speed of $v = 5225\,m/s$. Since this velocity is larger than the sound velocity of the gas ($c_{ideal} = 934\,m\,s^{-1}$* it can be assumed that his is the only relevant component of their velocity.

It is assumed that the gas source is located at the edge of the vessel, for this reason the direction of the velocity vector is chosen randomly according to a Knudsen cosine distribution [16]. This results in the spread of the velocity vector to be more focused normal to the edge, and less parallel to the plane. In figure 4.1 particles created by a puffing source are shown.

In order to test the validity of the puffing source, a source with a constant fueling rate has been modeled. The number of neutral particles in the simulation n_{puff} (for simplicity ionisation was not modeled) was tracked. This was compared with the expected number of particles $n_{theory} \equiv \texttt{fueling\_rate} \cdot t$. The error was calculated as

$$\epsilon_{puff} \equiv \left| 1 - \frac{n_{puff}}{n_{theory}} \right|. \tag{4.1}$$

In figure 4.2 the time evolution of ϵ_{puff} can be seen. Since the error is smaller than 10^{-4} it is considered negligible.

* The speed of the particles leaving the gas valve is assumed to be equal to the speed of sound of an ideal gas with temperature T and molecular mass m_{molec}:

$$c_{ideal} = \sqrt{\frac{\gamma \cdot k_B \cdot T}{m_{molec}}},$$

where γ is the adiabatic index. For diatomic deuterium $\gamma = 7/5$ and $m_{molec} = 2 \cdot 2\,u$, at room temperature ($T = 300\,K$), so $c_{ideal} = 934\,m\,s^{-1}$.

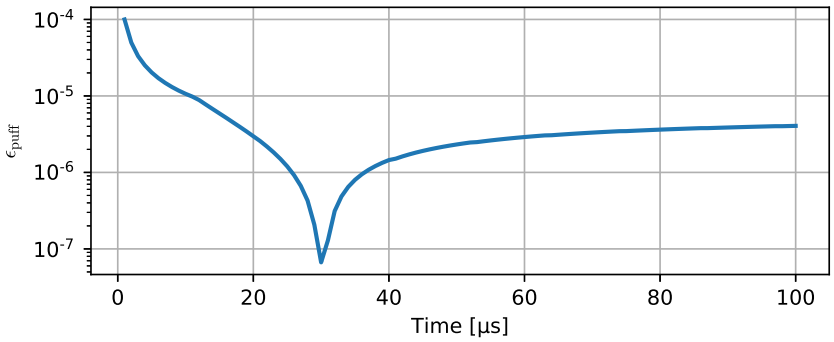

Figure 4.2: Error over time for particle source.

At the moment of writing the puffing source needs to be carefully placed. The normal to which the particle and velocity distribution is chosen is determined on the closest edge that can be found from the point that is specified to the code. This means that if the source is misplaced it would for send the particles with a velocity heading into the wall instead of the center of the plasma.

4.2 REFLECTION

When hydrogen ions hit the wall they can either be reflected or they will be implanted into the wall, until it is saturated. At the same when hydrogen ions recombine at the surface of the wall they return to the vessel [7]. After the recombination process the hydrogen molecule will diffuse out of the wall in to the vessel. Most likely it will subsequently dissociate into hydrogen atoms, which will get ionized. In order to implement reflection of particles, the sputtering module (as described in section 2.2.1) has been modified to allow for the 'sputtering' of deuterium. The sputtering module is mostly untouched but the sputtering yield and the energy of the returning particles are modified.

The sputtering yield is defined as the ratio of flux onto and off the wall, for reflection this ratio is set to 1. Thus all particles that hit the wall, will return to the vessel. This simulates the effect where the wall is fully saturated, which is usually the case for tokamak plasmas [7, p. 107]. Initially in order to limit complexity, the particles are returned as neutral atoms, not as neutral molecules. The energy of all reflected particles is set to be the energy of the particles will be assumed to be half of the dissociation energy of a D_2 atom: $2.28\,\text{eV}$ [27].

The wall can be changed to a sink by changing the reflection coefficient (i. e. the sputtering yield) to a value less then unity. A usage example could be having the walls of the vessel be fully reflective, but at the divertor change the reflection coefficient to be smaller to simulate the pumping that is implemented.

An example of a reflection source is shown in figure 4.3.

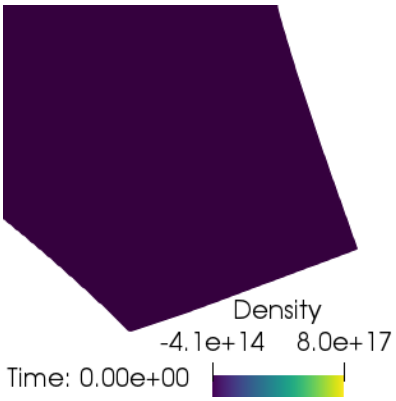

(a) At $t = 0\,\mu s$

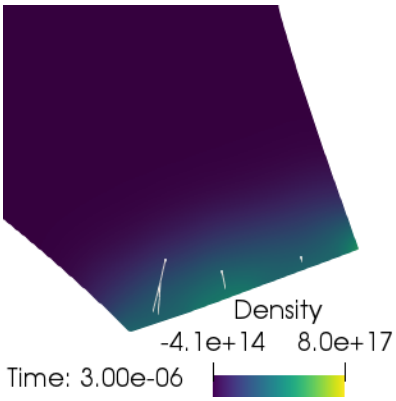

(b) At $t = 3\,\mu s$

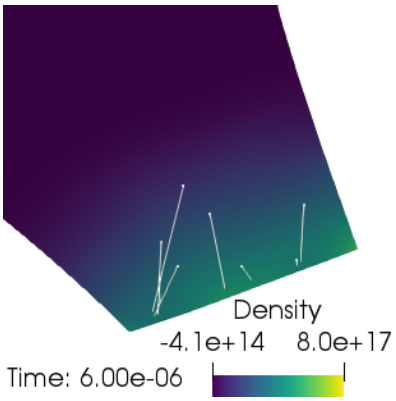

(c) At $t = 6\,\mu s$

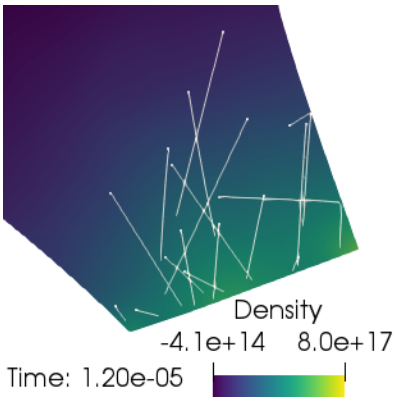

(d) At $t = 12\,\mu s$, note the particle reflection of tracked particles that bounce off the wall.

Figure 4.3: Visualisation of the reflection of the plasma flux at the outer divertor at different times. The particles are the white dots with their trails. The density projection at these times is the background of the plots.

5 COUPLING OF PARTICLE CODE TO JOREK

At the moment the JOREK code does not allow for the simulation of neutral particles in a particle like fashion. In order for the fluid code to take the physics of the particle code in to account the two need to be coupled. Because the neutral particles influence the plasma the coupling has to be done in simultaneous. For this the workflow (also visualized in figure 5.7) will be:

- A JOREK time step,
- Communicating the information of the plasma to the particle code,
- Multiple particle time steps,
- Communicating the information of the particles to the plasma code,
- another JOREK time step, repeating the process.

In this chapter the coupling between the main JOREK code and the particle extension will be explained, and an example run will be given.

As described in section 2.2, the particle code can read in the JOREK fields, but the information of the particle code could not influence a JOREK simulation yet. In order to achieve this, the particle code was coupled to JOREK to allow feedback.

The projection event described in section 2.2.2 can be used as a coupling mechanism from the particle code to JOREK, because the projection transforms the data from the particle code to the finite element description used by JOREK. This coupling was implemented but has limitations, mainly due to the snapshot nature of the projection function. The projection function determines the quantity that is to be projected from the parameters on the specific time that it is called. However when the time step between projections is too large, or the quantity that is to be projected changes quickly with time, discrepancies can occur.

An example of the snapshot behaviour is sketched in figure 5.1, here the decrease of a number of particles is shown. These particles are lost due to ionisation, and should be added as a source term to JOREK. The projection function assumes the amount of particles to be constant between the projection steps, resulting in the stepwise decreasing green dashed curve shown in the figure. Because of the difference between the two curves, the projection function underestimates the

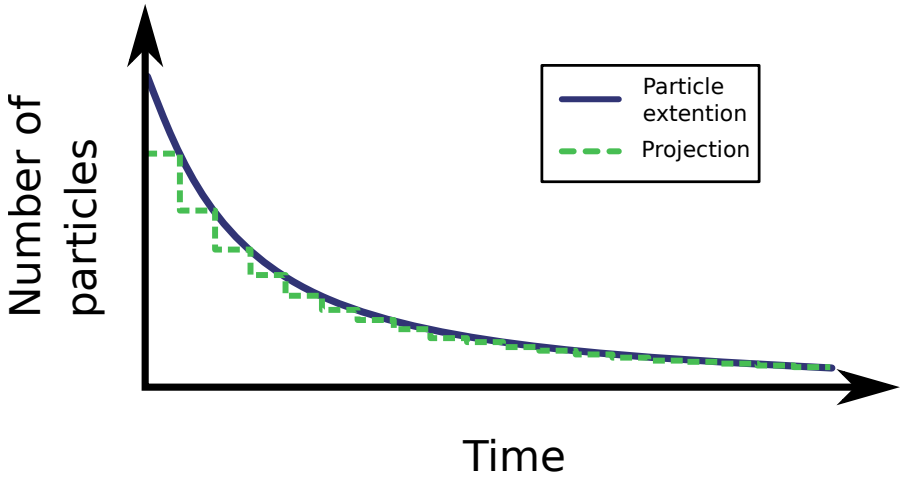

Figure 5.1: In blue a schematic representation of an amount of particles in the particle code is shown. The projection is done at regular intervals and the density that is used for the projection is shown in the green dashed curve. The projection function assumes the density to be constant over the interval, which is leads to errors when it changes rapidly like in the beginning.

source term in this case. By decreasing the time steps, this error can be reduced.

A more fundamental problem however, is that the conservation of mass between the particle code and JOREK is not guaranteed when using the projection function. When using the projection function the amount of particles lost due to ionisation are not recorded and only a guess on the parameters at the time of projection is used to add them to JOREK, thus not guaranteeing conservation of mass. By explicitly keeping track of the amount of particles lost (or other quantities) during particle stepping and adding them accordingly during a coupling event, conservation can be guaranteed. This cumulative summation of a source term will be explained using the example of density in section 5.2.1.

In this chapter first the different terms for feedback to JOREK or coupling terms are described. After that the implementation of a coupled run, i. e. running the particle code in tandem with JOREK, will be explained.

5.1 MHD EQUATIONS

The coupling sources that have been implemented are a density source S_n, an energy source S_K and a parallel momentum source $S_{p\parallel}$. The sources are added in blue to the relevant MHD equations [18]:

$$\frac{\partial \rho}{\partial t} + \nabla \cdot (\rho \vec{v}) = m S_n, \tag{5.1}$$

$$\frac{\partial \rho \vec{v}}{\partial t} + \nabla \cdot (\rho \vec{v} \vec{v}) + \nabla \cdot \overline{\overline{P}} = S_v, \tag{5.2}$$

$$\frac{\partial}{\partial t}\left(\frac{1}{2}\rho v^2 + \frac{3}{2}\rho T\right) + \nabla \cdot \left(\frac{1}{2}\rho v^2 \vec{v} + \frac{3}{2}\rho T \vec{v} + \vec{v} \cdot \overline{\overline{P}}\right) = S_K. \tag{5.3}$$

With the pressure tensor $\overline{\overline{P}}$. These can be rewritten for JOREKfor the parallel velocity* and energy equations (note the density equations stays unchanged):

$$\rho \frac{\partial v_\parallel}{\partial t} + \rho \left(\nabla v_\parallel\right) v_\parallel + \nabla \cdot \overline{\overline{P}} = S_{v\parallel} - v_\parallel S_n \tag{5.4}$$

$$\frac{\partial \frac{3}{2}\rho T}{\partial t} + v_\parallel \cdot \nabla \left(\frac{3}{2}\rho T\right) + \frac{5}{2}\rho T \left(\nabla v_\parallel\right) = S_K - v_\parallel S_{v\parallel} + \frac{1}{2} v_\parallel^2 S_n \tag{5.5}$$

5.2 COUPLING TERMS

The coupling terms that have been implemented are a density (n), energy (K) and a parallel momentum ($p_\parallel$) term. Even though recombination has not been implemented its contributions will be shown. For ionisation, charge exchange and recombination these terms are shown in table 5.1. The sources described in the previous section can be found when summing over the entries of each row of this table, so for density this is $S_n = R_\mathrm{i}(n_e, T_e) n_e + 0 + R_\mathrm{re}(n_e, T_e) n_e$.

Table 5.1: Coupling terms from particle code to JOREK.

	Ionisation	Charge Exchange	Recombination
n	$R_\mathrm{i}(n_e, T_e) n_e$	0	$R_\mathrm{re}(n_e, T_e) n_e$
K	$\left(\frac{1}{2}mv^2 - \varepsilon\right) S_{n,\mathrm{i}}$	$\frac{1}{2} m \Delta v^2 S_{n,\mathrm{CX}}$	$-\frac{1}{2} m v^2 S_{n,\mathrm{re}}$
$p_\parallel$	$m\vec{v} \cdot \hat{B} S_{n,\mathrm{i}}$	$m\left(\Delta \vec{v}\right) \cdot \hat{B} S_{n,\mathrm{CX}}$	$-m\vec{v} \cdot \hat{B} S_{n,\mathrm{re}}$

Here $S_{n,\mathrm{X}}$ is a source, for example $S_{n,\mathrm{i}} = R_\mathrm{i}(n_e, T_e) n_e$ is the ion source. The subscripts i, CX and re stand for ionisation, charge exchange and recombination respectively. In the charge exchange column

$$\Delta v^2 = v_1^2 - v_2^2, \tag{5.6}$$

where v_1 is the velocity of the particle before it undergoes the charge exchange and v_2 is the velocity it has after the charge exchange event. The direction of the magnetic field is denoted

$$\hat{B} = \frac{\vec{B}}{|\vec{B}|}. \tag{5.7}$$

* The parallel velocity is the velocity along the magnetic field, so $v_\parallel = \vec{v} \cdot \hat{B}$

5.2.1 *Density*

In section 3.1 the process of ionisation of particles is described, during each particle step the amount of physical particles is projected to the density source term. After the particle stepping has completed the source term is added to the JOREK equations during a feedback step. The process for ionisation, as implemented in the code, can be found in listing 5.1.

On the first line the ion source (i. e. the number of physical particles that have been removed due to ionisation in the particle stepping, visualized in figure 3.2) is normalized. Before projection the number of particles is dimensionless, due to how the projection is implemented, it will be transformed into a number density source with units $\mathrm{m}^{-3}\mathrm{s}^{-1}$. This needs to be normalized to JOREK units by multiplying with a factor of

$$\frac{\sqrt{\rho_0 \mu_0}}{n_0}.$$

The basis functions HH, and their derivatives, and the 'toroidal basis functions' HZ are then calculated. After that a loop over 3 variables is started:

- `l` denotes the vertex of the final element.
- `m` denotes which basis function is to be used.
- `i_tor` denotes which toroidal harmonic is to be used.

The contribution of the source (`HZ(i_tor) * v`) is determined by multiplying it with the basis functions (including the toroidal basis functions) and the size of the element.

Listing 5.1: Density coupling

```
1  ion_source = ion_source * sqrt((MU_ZERO * CENTRAL_MASS *
       MASS_PROTON) / (CENTRAL_DENSITY * 1.d20))
2  call basisfunctions(particles(j)%st(1), particles(j)%st(2), HH,
       HH_s, HH_t)
3  call mode_moivre(particles(j)%x(3), HZ)
4  HZ(1) = HZ(1)*0.5d0 ! int cos^2(nx) from 0 to 2pi = pi for n > 0
5  HZ(:) = HZ(:)/PI ! int 1 from 0 to 2pi = 2pi
6  do l=1,n_vertex_max
7    do m=1,n_order+1
8      v = HH(l,m) * sim%fields%element_list%element(i_elm_old)%size
           (l,m) * ion_source
9      do i_tor=1,n_tor
10       !$omp atomic
11       jorek_feedback%rhs(m,l,i_elm_old,i_tor,1) = &
12       jorek_feedback%rhs(m,l,i_elm_old,i_tor,1) + HZ(i_tor) * v
13     enddo
14   enddo
15 enddo
```

In order to check density conservation 10^{20} particles were placed in a simple circular equilibrium, which ionize. When ionizing the particles should be added to the JOREK density. The number of particles in the particle extension (N_{par}) and the added JOREK equilibrium (N^*_{jor}) are shown in figure 5.3, which are normalized by dividing them by 10^{20}. Also the sum of these N_{con}, which shows the conservation of particles, can be seen in the figure. Finally the error

$$\varepsilon_{\text{ion}} = \left|1 - N_{\text{par}} - N^*_{\text{jor}}\right|, \tag{5.8}$$

is also plotted. Since this error is not much greater then 10^{-4} it can be concluded that the conservation of particles is in order.

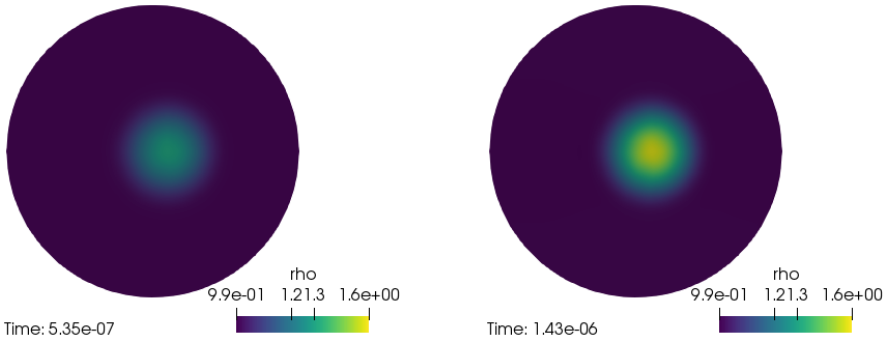

(a) At $t = 5.35\,\mu\text{s}$ (b) At $t = 1.43\,\mu\text{s}$

Figure 5.2: Figures of ρ resulting from the particle distribution of the particle conservation test during coupling at different times.

5.2.2 *Energy*

The energy source of ions is given by the difference of the kinetic energy of the neutrals minus the energy that is needed to ionise them. This is scaled with the ion source term, so that the energy added is proportional to the amount of particles that are ionized.

$$S_{K,\text{i}} = \left(\frac{1}{2}mv^2 - \varepsilon\right) S_{n,\text{i}}. \tag{5.9}$$

Here we assume all atoms are in the ground state, i.e. the binding energy for all particles is $\varepsilon = 13.6\,\text{eV}$.

The energy source for charge exchange is given by the difference of the velocity of the particles $\vec{v}_{\text{par}}$ and the average plasma velocity $\vec{v}_{\text{pla}}$:

$$S_{K,\text{CX}} = \frac{1}{2}m\Delta v^2 S_{n,\text{CX}}, \tag{5.10}$$

where $\Delta v \equiv \vec{v}_{\text{par}} - \vec{v}_{\text{pla}}$.

The energy projection was tested by creating an energy source with a strength of $P_{\text{source}} = 1\,\text{GW}$. Two simulations were run, one plain (i. e.

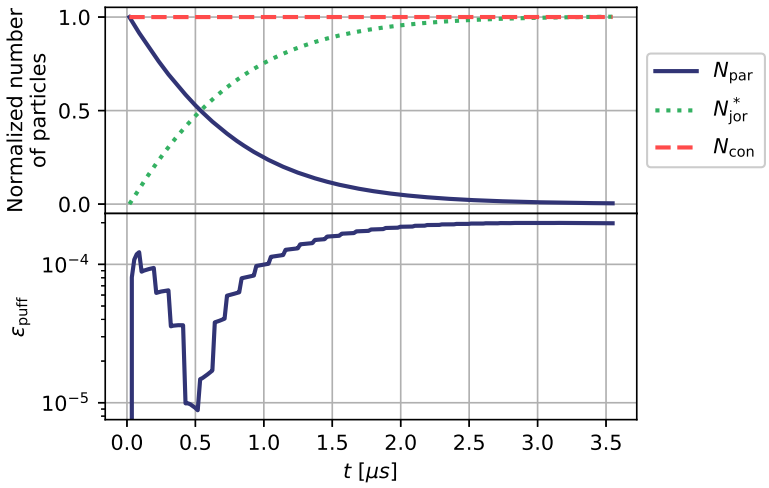

Figure 5.3: In this figure the particle conservation is shown. A total of 1×10^{20} neutrals were added to a jorek equilibrium. The top graph shows the normalized number of particles for the particle extension, the particles added to JOREK, and the sum of those (in solid blue, green dotted and red dashed respectively).
The bottom plot shows the error ε_{ion} in the particle conservation.

without the source) and one with the source. In these simulations the total amount of energy in the plasma was being kept track of $E_{\text{tot,w}}$ and $E_{\text{tot,p}}$ for the run with and without the source respectively. The difference $E^*_{\text{tot}} = E_{\text{tot,w}} - E_{\text{tot,p}}$ yields the energy that is added to the plasma by the source, it should be the same as the theoretical energy increase $E_{\text{theory}} = P_{\text{source}} \cdot t$. The error of the energy source is given by:

$$\varepsilon_{\text{energy}} = \left| 1 - \frac{E^*_{\text{tot}} - E_{\text{theory}}}{E_{\text{theory}}} \right| \tag{5.11}$$

The result of the simulation is shown in figure 5.4. From this figure it can be seen that the simulated energy source is to small at the beginning but later on adjusts to the correct value. The error stays quite large at almost reaching 10^{-2}. So the coupling works to some extent but needs to be improved.

5.2.3 *Momentum*

Momentum conservation in a coupled run will be treated as the conservation of particles as shown in section 5.2.1. Again 10^{20} particles are brought into a JOREK equilibrium. The particles will be initialized with a set parallel velocity, which due to ionisation will be transferred to the plasma. The quantities that are being tracked are the parallel momentum of the particles $p_{\parallel,\text{par}}$ and the parallel momentum added

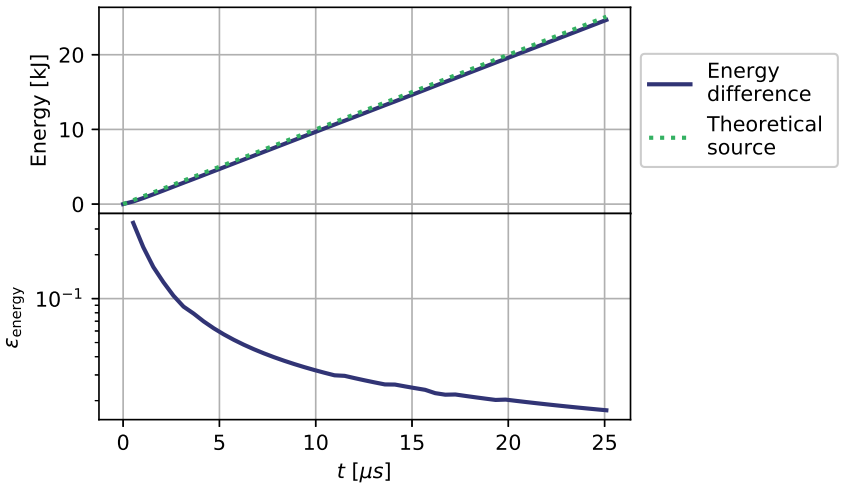

Figure 5.4: The energy increase of the plasma due to a power source is plotted. In the top plot different energies over time are plotted. The blue solid line shows the energy added to the JOREK plasma, E^*_{tot}. The green dotted line shows the theoretical prediction for energy increase E_{theory} and matches with the observed behaviour. In the lower plot the error $\varepsilon_{\text{energy}}$ is shown.

to the plasma $p^*_{\parallel,\text{jor}}$, from which the conservation $p_{\parallel,\text{con}} = p_{\parallel,\text{par}} + p^*_{\parallel,\text{jor}}$ and the error therein

$$\varepsilon_{p\parallel} = \left| 1 - p_{\parallel,\text{par}} - p^*_{\parallel,\text{jor}} \right|, \tag{5.12}$$

can be calculated.

5.3 COUPLED RUN

In order to improve the SOL models in JOREK the particle code and JOREK should be run in tandem, while they communicate and update each others data. The schematic representation of this coupling in shown in figures 5.6 and 5.7. Because particle codes work on smaller timescales there will be particle steps in between JOREK. The amount of particle steps that will be interjected depend on the particular phenomena to be researched. Some will demand for small JOREK time steps resulting in fewer particle steps, whilst others will not require a high temporal resolution for the particles thus increasing the amount of particle steps needed.

5.3.1 *Time stepping*

To determine the amount of particle steps to be taken until the next event the following algorithm (for which the variables are visualized in figure 5.6) is followed.

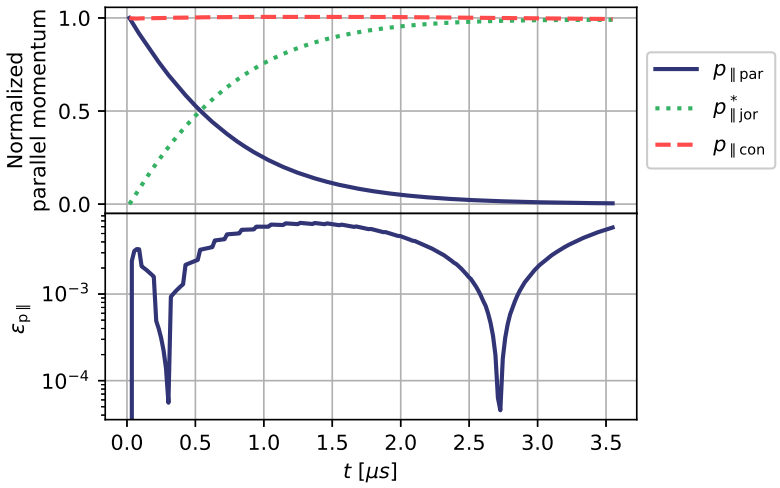

Figure 5.5: In this figure parallel momentum conservation is shown. A total of 1×10^{20} neutrals were added to a jorek equilibrium. The top graph shows the normalized parallel momentum for the particle extension, the parallel momentum added to the JOREK plasma, and the sum of those (in solid blue, green dotted and red dashed respectively).
The bottom plot shows the error $\varepsilon_{p\parallel}$ in the parallel momentum conservation.

Listing 5.2: Time synchronisation

```
1 particle_start_time = (sim%time - step_rest_time)
2 particle_step_time = target_time - particle_start_time
3 n_steps = particle_step_time/timesteps
4 step_rest_time = particle_step_time - real(n_steps,8) * timesteps
```

The variables of this algorithm are shown in figure 5.6 for the case where the only events are JOREK coupling steps.

Of special interest is the division in line 3, this is integer division (a flooring operation), since generally time between JOREK steps is not divisible by the size of the particle time steps. The remainder of this division is represented by the `step_rest_time`, which means that the at the desired JOREK time the particle simulation is slightly behind. This underestimation can be reduced by increasing the number of particle steps to be taken in between events. This problem can be avoided if the JOREK step time is a multiple of the particle step time (i. e. $\Delta t_{\mathrm{jorek}} = N \cdot$ `timesteps`), but one also has to take into account the time steps of the other events that are planned.

The particle time step size is limited by the time it takes for the neutrals to traverse the typical length scale discussed in section 1.4.1 $l \approx 1\,\mathrm{mm}$. The highest velocity the neutrals will have is determined by the velocity they can have after a charge exchange event, which is dependent on the temperature of the plasma, which is in the order of $T_e \approx 1\,\mathrm{keV}$. If it assumed that the velocity of the plasma particles is

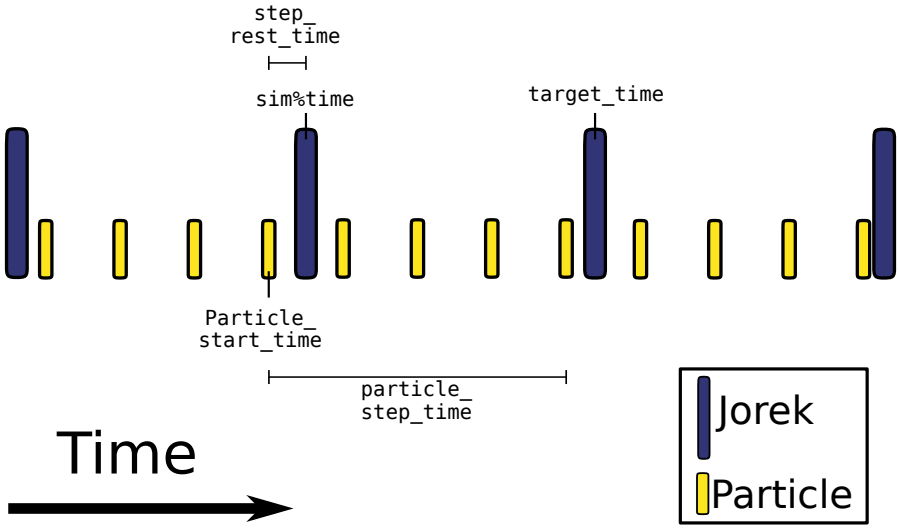

Figure 5.6: Schematic representation of a coupled run. Each block represents a computational step, blue if it is a JOREK step, yellow if it is a particle step. Due to the nature of the computational methods the time step for particle steps is smaller then those for JOREK steps, resulting in a multitude of particle steps between the JOREK steps. The annotations are the variables as described in listing 5.2, for the particle steps between the second and third JOREK time step.

distributed with a Maxwell–Boltzmann distribution and we want to take into account two times the standard deviation (σ), the speed of the particle with the largest velocity that will be taken into account is:

$$v_{\max} = \sqrt{\frac{3k_{\mathrm{B}}T_e}{m}} + 2\sigma = 3\sqrt{\frac{3k_{\mathrm{B}}T_e}{m}} \approx 1.1 \times 10^6\,\mathrm{m/s}. \tag{5.13}$$

With this velocity and the typical length scales it can be shown that the time steps for the particles should not be larger then $\texttt{timesteps}_{\max} \approx 1\,\mathrm{ns}$.

5.3.2 *Example run*

An example case was run. For this case a JET equilibrium was time evolved in JOREK coupled to a particle simulation where the wall was made fully reflective (as per section 4.2), and the neutrals could ionize and charge exchange (as explained in chapter 3). The results of this are shown in the following figures. In these figures only the bottom half of the vessel is shown, as most neutrals are born on the divertor plates (where plasma flux, thus reflection, is strongest).

At first JOREK was run without the particle code to allow for a equilibrium to form. The initial state of this equilibrium is shown in figure 5.8. At $t = 1.57\,\mu\mathrm{s}$ the particle code and coupling were switched on. The simulation was terminated after about $500\,\mu\mathrm{s}$.

The only source is the reflection source, and because the flux of plasma is largest directly on the divertor the main most neutrals

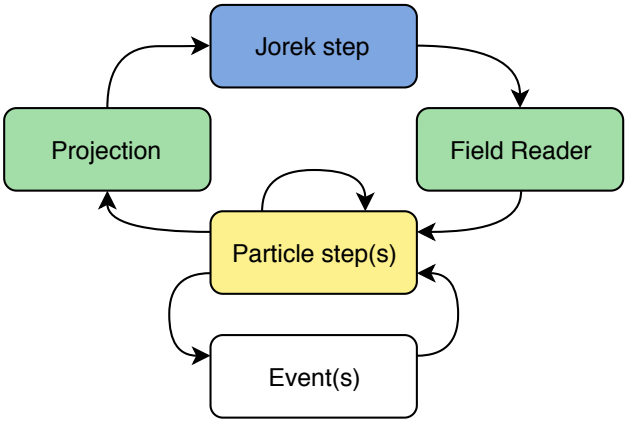

Figure 5.7: Workflow for a coupled run. Between the JOREK and particle steps communication is implemented (green blocks). After a JOREK step the new fields are read in by the particle code by using the field reader event. After the particle steps the information is projected onto JOREK space and added to the right hand sides of the MHD equations.
Also other events can be run, such as diagnostics.

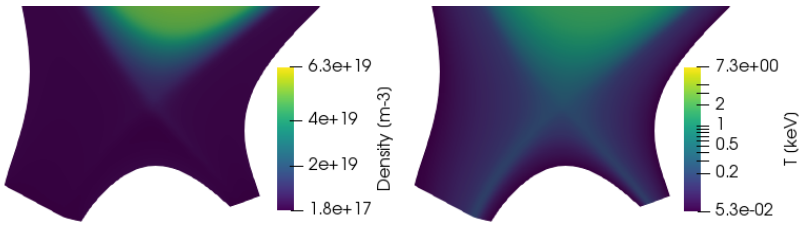

(a) Plasma density in m^{-3} (b) Temperature in keV

Figure 5.8: Initial state of the plasma for density and temperature in the divertor region.

originate from the divertor plates. This can be seen in figure 5.9, which depicts the density source. The particles that originate from the divertor form a front that moves inward to the vessel. Ahead of the front there are neutrals that traveled faster inward due to the charge exchange events. After about $100\,\mu\mathrm{s}$ the source doesn't change anymore.

Even though the density source seems stable, at the end of the simulation the neutral distribution appears to oscillate when moving from the divertor towards the center of the vessel, as can be seen in figure 5.10. This is because the time interval for the reflection source was chosen to long: it periodically injects neutral particles, which move away from the divertor before a new generation has been created.

Also the divertor density is not stable at the end of the simulation. It has been doubling in the time that the simulation has started as can been seen in figure 5.11. No non-negligible change in the temperature or other plasma parameters have been observed.

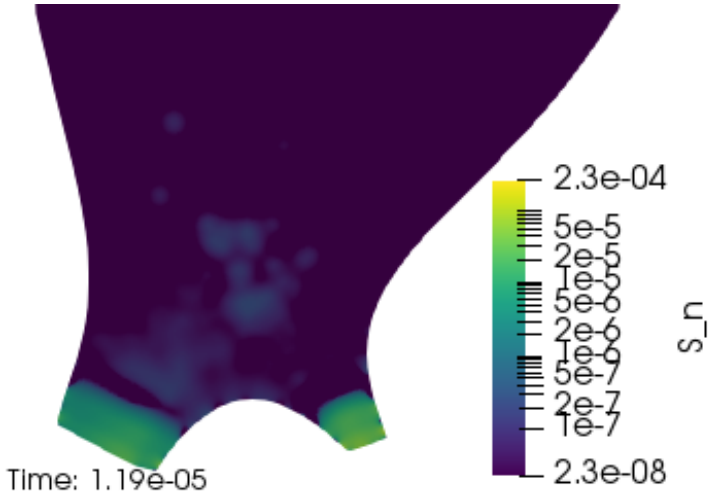

(a) At $t = 11.9\,\mu s$

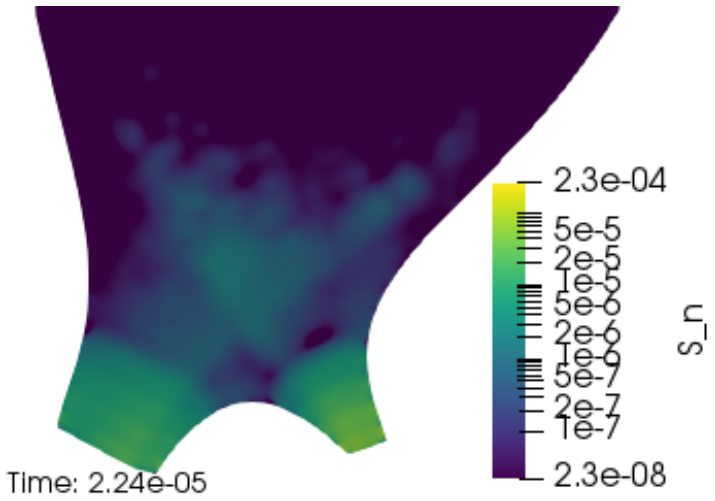

(b) At $t = 22.4\,\mu s$

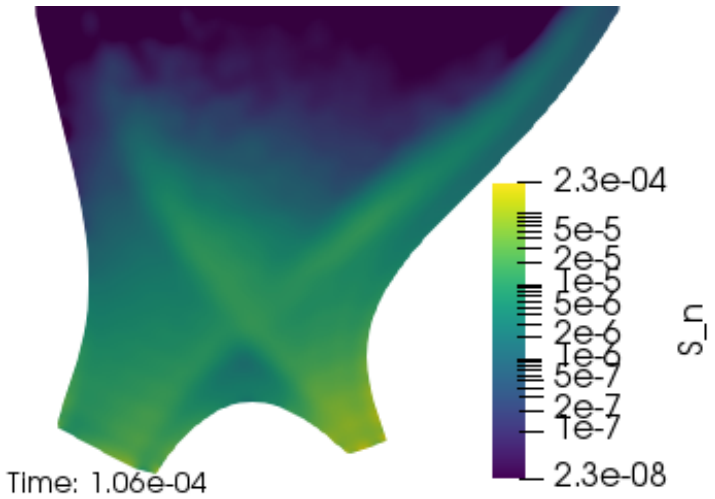

(c) At $t = 106\,\mu s$

Figure 5.9: Time evolution of the density source

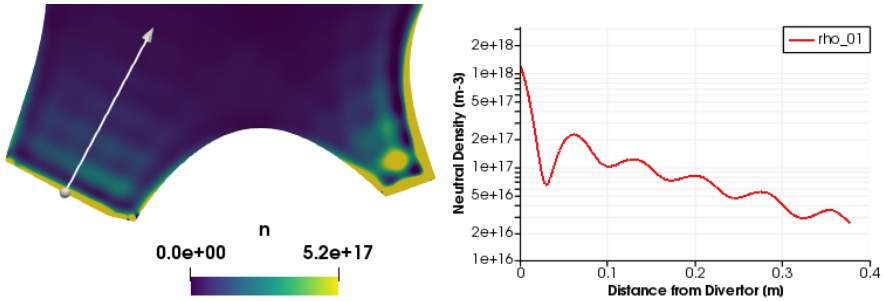

Figure 5.10: Neutral distribution at the end of the simulation in the divertor (left). There is an oscillatory behaviour because of the reflection source.
The right figure shows the density along the arrow shown in the left figure, traveling towards the center of the vessel.

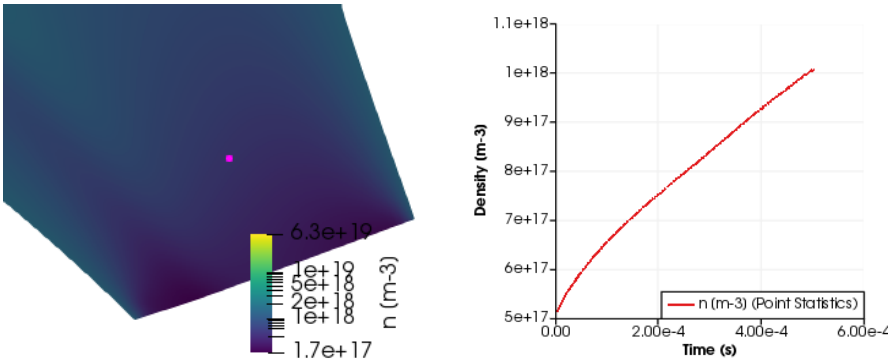

(a) Outer divertor leg with the magenta dot on the probing location.

(b) Neutral density over time at the probing location.

Figure 5.11: Neutral density in the outer divertor leg over time.

6 CONCLUSION AND FUTURE WORK

The JOREK particle extension has been expanded to include neutral particles. Two sources of neutral particles have been developed. The first being a puffing source that can be used as a circular 2D source or a 3D toroidal source. The second is a source reflecting particles from the wall. The strength of this reflection source is determined by both the flux of plasma on the wall and the amount of neutral particles hitting the wall.

The physics of the neutrals that has been implemented includes charge exchange events and ionisation. The feedback of the neutral particles on the main MHD code has been implemented. This feedback has been realized for the density, parallel momentum and energy MHD equations.

With the already existing feedback of the plasma on the particle code, a coupling between the two can be made. This coupling has been developed and allows for runs of the JOREK code together with the particle extension, each giving feedback to each other.

The sources and coupling has been verified and shown to work as intended. A straightforward example run has been shown. This example run shows little deviation from the equilibrium for most of the plasma parameters. An exception is the plasma density in the divertor region that increase. The density was still increasing at the end of the simulation, so longer simulations are needed to show steady-state behaviour.

6.1 FEATURES TO BE IMPLEMENTED

The following features can be included to allow for a more thorough and solid code. A major feature that should be included is the radiation of neutral particles. This mechanism plays a large role in the formation of a detached plasma.

Another element which probably will be needed for detachment is recombination. Although it is described in this thesis, but has not been implemented. Its implementation would require a sink in the MHD code and a source for the particle extension.

For the calculation of the particle and energy reflection coefficients, which are now set to hard coded values, the TRIM code could be used. This would call for a separate reflection module, instead of the current modified use of the sputtering module.

At the moment the assumption that the neutral sources bring in hydrogen atoms is quite crude. The simulations can be refined and

more realistic when the behaviour of atomic hydrogen and its physics is implemented.

6.2 FUTURE APPLICATIONS

The JOREK code with the particle extension and neutrals particles, when further developed with the suggestions given above, can be used to simulate MHD behaviour of plasma in a tokamak. It can be used for simulating detachment and also ELM behaviour in such a detached plasma. Also the physics of different fueling mechanisms can be researched, such as fueling by neutral beam injection or edge fueling. Other uses could be simulating techniques that are used to terminate the plasma when a disruption is imminent such as massive gas injections and shattered pellet injections.

BIBLIOGRAPHY

[1] Kerstine Appunn. *The history behind Germany's nuclear phase-out*. 2018. URL: https://www.cleanenergywire.org/factsheets/history-behind-germanys-nuclear-phase-out (visited on 18/02/2018).

[2] Francisco Javier Artola. 'Free-boundary simulations of MHD plasma instabilities in tokamaks'. PhD thesis. Aix-Marseille Université, 2018, pp. 1–51. URL: https://tel.archives-ouvertes.fr/tel-02012234.

[3] C.K. Birdsall and A.B. Langdon. *Plasma Physics via Computer Simulation*. New York: CRC Press, Oct. 2004, p. 504. ISBN: 9781482263060. DOI: 10.1201/9781315275048. URL: https://www.taylorfrancis.com/books/9781482263060.

[4] Xavier Bonnin, Wouter Dekeyser, Richard Pitts, David Coster, Serguey Voskoboynikov and Sven Wiesen. 'Presentation of the New SOLPS-ITER Code Package for Tokamak Plasma Edge Modelling'. In: *Plasma and Fusion Research* 11.0 (2016), pp. 1403102–1403102. ISSN: 1880-6821. DOI: 10.1585/pfr.11.1403102. URL: https://www.jstage.jst.go.jp/article/pfr/11/0/11%7B%5C_%7D1403102/%7B%5C_%7Darticle.

[5] P. Cahyna, M. Peterka, A. Kirk, A. Thornton, J. Harrison, D. Muir and R. Panek. 'Strike point splitting induced by the application of magnetic perturbations on MAST'. In: *Journal of Nuclear Materials* 438.SUPPL (2013), S326–S329. ISSN: 00223115. DOI: 10.1016/j.jnucmat.2013.01.060. URL: http://dx.doi.org/10.1016/j.jnucmat.2013.01.060.

[6] Niek Lopes Cardozo. *Fusion on the back of an envelope, Lecture Notes*. 2018.

[7] Rion A. Causey. 'Hydrogen isotope retention and recycling in fusion reactor plasma-facing components'. In: *Journal of Nuclear Materials* 300.2-3 (2002), pp. 91–117. ISSN: 00223115. DOI: 10.1016/S0022-3115(01)00732-2.

[8] Centraal Bureau voor de Statistiek. *Cijfers - Energie*. 2018. URL: https://longreads.cbs.nl/trends18/economie/cijfers/energie/ (visited on 18/02/2019).

[9] Centraal Bureau voor de Statistiek. *Energiebalans; aanbod, omzetting en verbruik*. 2019. URL: https://opendata.cbs.nl/statline/%7B%5C#%7D/CBS/nl/dataset/83140NED/table?dl=19CE2 (visited on 18/02/2019).

[10] Sydney Chapman and T. G. Cowling. *The Mathematical Theory of Non-uniform Gases: An Account of the Kinetic Theory of Viscosity, Thermal Conduction and Diffusion in Gases*. Ed. by D. Burnet. Third edit. Cambridge: Cambridge University Press, 1990, p. 423. ISBN: 9780521408448.

[11] Eric G Chipman, Bevan M. French., Donald L. De Vincenzi, David Gilman, Stephen P. Maran and Paul C. Rambaut. *A Meeting with the Universe: Science Discoveries from the Space Program*. Washington, DC: GPO, 1981. URL: https://history.nasa.gov/EP-177/toc.html.

[12] Olivier Czarny and Guido Huysmans. 'Bézier surfaces and finite elements for MHD simulations'. In: *Journal of Computational Physics* 227.16 (2008), pp. 7423–7445. ISSN: 00219991. DOI: 10.1016/j.jcp.2008.04.001.

[13] T. Eich et al. 'Scaling of the tokamak near the scrape-off layer H-mode power width and implications for ITER'. In: *Nuclear Fusion* 53.9 (Sept. 2013), p. 093031. ISSN: 0029-5515. DOI: 10.1088/0029-5515/53/9/093031. URL: http://stacks.iop.org/0029-5515/53/i=9/a=093031?key=crossref.85c8939d5380098d23c4644a2a101ec9.

[14] J P Freidberg. *Plasma physics and fusion energy*. Vol. 1. 2007, p. 671. ISBN: 0521851076. DOI: 10.2277/0521851076. arXiv: arXiv:1011.1669v3.

[15] Clair Gavin. *GB Electricity Demand Profiles , Summer vs Winter*. Tech. rep. March. United Kingdom Department of Energy & Climate Change, 2014. URL: https://www.gov.uk/government/uploads/system/uploads/attachment%7B%5C_%7Ddata/file/295225/Seasonal%7B%5C_%7Dvariations%7B%5C_%7Din%7B%5C_%7Delectricity%7B%5C_%7Ddemand.pdf.

[16] John Greenwood. 'The correct and incorrect generation of a cosine distribution of scattered particles for Monte-Carlo modelling of vacuum systems'. In: *Vacuum* 67.2 (2002), pp. 217–222. ISSN: 0042207X. DOI: 10.1016/S0042-207X(02)00173-2.

[17] Emiel Hakkenes. *Nederlandse vissers voelen zich van de Noordzee verdreven - en dat pikken ze niet langer*. 2018. URL: https://www.trouw.nl/groen/nederlandse-vissers-voelen-zich-van-de-noordzee-verdreven-en-dat-pikken-ze-niet-langer%7B~%7Da36aa99e/.

[18] Guido Huijsmans. 'ELMs in Detached ITER Plasmas'. In: *Jorek meeting 2019*. Garching, 2019.

[19] G. T A Huysmans and O. Czarny. 'MHD stability in X-point geometry: Simulation of ELMs'. In: *Nuclear Fusion* 47.7 (2007), pp. 659–666. ISSN: 00295515. DOI: 10.1088/0029-5515/47/7/016.

[20] ITER. *Facts & Figures*. 2018. URL: https://www.iter.org/FactsFigures (visited on 25/02/2019).

[21] ITER Physics Expert Groups on Confinement and Trasport and Confinement Modelling and Database. 'Chapter 2 : Plasma confinement and transport ITER Physics Expert Groups on Confinement and Transport and Confinement Modelling and Database'. In: *Nuclear Fusion* 39.12 (1999).

[22] Tao Jiang, Bo Li, Wei Li, Mingxu Wang, Yudong Pan, So Maruyama and Yu Yang. 'Manifold concept design for ITER gas injection system'. In: *IEEE Transactions on Plasma Science* 40.3 PART 1 (2012), pp. 788–792. ISSN: 00933813. DOI: 10.1109/TPS.2012.2185718.

[23] S. Q. Korving. *Implementation and verification of a sputtering model in the non-linear MHD code JOREK*. 2018.

[24] S. I. Krasheninnikov, A. S. Kukushkin and A. A. Pshenov. 'Divertor plasma detachment'. In: *Physics of Plasmas* 23.5 (2016). ISSN: 10897674. DOI: 10.1063/1.4948273.

[25] S. I. Krasheninnikov, A. Yu Pigarov and D. J. Sigmar. 'Plasma Recombination and Divertor Detachment'. In: *Contributions to Plasma Physics* 36.2-3 (1996), pp. 314–318. ISSN: 08631042. DOI: 10.1002/ctpp.2150360239.

[26] Bradley E. Layton. 'A comparison of energy densities of prevalent energy sources in units of joules per cubic meter'. In: *International Journal of Green Energy* 5.6 (2008), pp. 438–455. ISSN: 15435075. DOI: 10.1080/15435070802498036.

[27] Jinjun Liu, Daniel Sprecher, Christian Jungen, Wim Ubachs and Frédéric Merkt. 'Determination of the ionization and dissociation energies of the deuterium molecule (D2)'. In: *The Journal of Chemical Physics* 132.15 (Apr. 2010), p. 154301. ISSN: 0021-9606. DOI: 10.1063/1.3374426. URL: http://aip.scitation.org/doi/10.1063/1.3374426.

[28] N. J. Lopes Cardozo, A. G.G. Lange and G. J. Kramer. 'Fusion: Expensive and Taking Forever?' In: *Journal of Fusion Energy* 35.1 (2016), pp. 94–101. ISSN: 01640313. DOI: 10.1007/s10894-015-0012-7.

[29] D J C Mackay. *Sustainable Energy - without the hot air. Version 3.5.2. November 3, 2008*. 2008, p. 382. ISBN: 978-0954452933. DOI: 10.1109/PES.2004.1373296.. arXiv: arXiv:1011.1669v3. URL: https://www.withouthotair.com/.

[30] V. Masson-Delmotte et al. *Global Warming of 1.5°C*. Tech. rep. IPCC, 2018. URL: https://www.ipcc.ch/report/sr15/.

[31] Tim Meulenbroeks. *Deuterium Tritium Fusion*. (Personal communication), 2018.

[32] Tim Meulenbroeks. *Tokamak schematic*. (Personal communication), 2018.

[33] Bruce R. Munson, Theodore H. Okiishi, Wade W. Huebsch and Alric P. Rothmayer. *Fundamentals of Fluid Mechanics*. 7th ed. Jefferson City: John Wiley & Sons, Inc., 2013. ISBN: 978-1-118-11613-5. URL: https://www.wiley.com/en-us/Fundamentals+of+Fluid+Mechanics%7B%5C%%7D2C+7th+Edition-p-ES81118116135.

[34] NOS. *Steeds vaker verzet tegen windmolens*. 2016. URL: https://nos.nl/l/2078831 (visited on 27/02/2019).

[35] NOS. *In Gelderland merken ze: energiebedrijven hebben landhonger om zonnepanelen*. 2019. URL: https://nos.nl/l/2274449 (visited on 04/03/2019).

[36] Omroep West. *Actiegroepen protesteren tegen 'horizonvervuiling' door windmolenparken in Noordzee: 'Er zijn alternatieven'*. 2015. URL: http://owst.nl/57yo (visited on 18/02/2018).

[37] Daniel V. Schroeder. *An introduction to thermal physics*. San Francisco, CA: Addison Wesley, 2000, p. 422. ISBN: 978-0201380279.

[38] Jacob Schwartz. *Atomic*. 2019. URL: https://github.com/cfe316/atomic (visited on 20/09/2003).

[39] Solarcentury. *Zonnepark Budel*. 2018. URL: https://www.solarcentury-zonneparken.com/zonnepark-budel/ (visited on 18/02/2018).

[40] Anitha S. Subburaj, Bejoy N. Pushpakaran and Stephen B. Bayne. 'Overview of grid connected renewable energy based battery projects in USA'. In: *Renewable and Sustainable Energy Reviews* 45 (May 2015), pp. 219–234. ISSN: 13640321. DOI: 10.1016/j.rser.2015.01.052. URL: https://linkinghub.elsevier.com/retrieve/pii/S1364032115000623.

[41] The ADAS Project. *OPEN-ADAS*. 2019. URL: http://open.adas.ac.uk/ (visited on 04/03/2019).

[42] Janos Timar, Zoltan Elekes and Balraj Singh. *Nuclear Data Sheets 121, I-129 Decay Radiation*. Brookhaven, 2014. URL: https://www.nndc.bnl.gov/chart/decaysearchdirect.jsp?nuc=129I%7B%5C&%7Dunc=nds.

[43] Top500. *The List, November*. 2018. URL: https://www.top500.org/lists/2018/11/ (visited on 25/02/2018).

[44] U.S. Energy Information Administration. *Electric Power Monthly with Data for July 2015*. Tech. rep. January. 2019. URL: https://www.eia.gov/electricity/monthly/.

[45] United States Nuclear Regulatory Commission. *Radioactive Waste High-Level Waste*. Tech. rep. 2015, pp. 1–5. URL: https://www.nrc.gov/reading-rm/doc-collections/fact-sheets/radwaste.pdf.

[46] United States Nuclear Regulatory Commission. *Capacity factor (net)*. 2018. URL: https://www.nrc.gov/reading-rm/basic-ref/glossary/capacity-factor-net.html (visited on 20/02/2019).

[47] D. C. van Vugt. 'Nonlinear coupled MHD-kinetic particle simulations of heavy impurities in tokamak plasmas'. PhD thesis. Eindhoven University of Technology, 2019.

[48] Daan Van Vugt and Guido Huijsmans. *Deliveralbe 1: Implementation of test particle model for W expulsion by ELMs and experimental validation.* Tech. rep. 1. 2017.

[49] S. Wiesen et al. 'The new SOLPS-ITER code package'. In: *Journal of Nuclear Materials* 463 (2015), pp. 480–484. ISSN: 00223115. DOI: 10.1016/j.jnucmat.2014.10.012. URL: http://dx.doi.org/10.1016/j.jnucmat.2014.10.012.

[50] World Nuclear Association. *Generation IV Nuclear Reactors*. Tech. rep. 2017. URL: http://www.world-nuclear.org/information-library/nuclear-fuel-cycle/nuclear-power-reactors/generation-iv-nuclear-reactors.aspx.

[51] World Nuclear Association. *Radioactive Waste Management*. 2018. URL: http://www.world-nuclear.org/information-library/nuclear-fuel-cycle/nuclear-wastes/radioactive-waste-management.aspx.

Part I

APPENDIX

A

JOREK EQUATIONS AND VARIABLES

A.1 JOREK EQUATIONS

The JOREK equations for model 303 are shown below, addition for model 307 are done in blue:

$$\frac{\partial \rho}{\partial t} = -\rho\left(-2\frac{\partial u}{\partial Z} + \frac{1}{R}[v_\parallel, \psi] + \frac{F_0}{R^2}\frac{\partial v_\parallel}{\partial \phi}\right) + R[\rho, u] - v_\parallel\left(\frac{1}{R}[\rho, \psi] + \frac{F_0}{R^2}\frac{\partial \rho}{\partial \phi}\right) + \nabla\cdot(D_\perp \nabla_\perp \rho) + S_\rho + S_n \quad \text{(A.1)}$$

$$\rho B^2 \frac{\partial v_\parallel}{\partial t} + \frac{1}{R^2}\rho v_\parallel \nabla_{pol}\psi\cdot\nabla_{pol}\frac{\partial \psi}{\partial t} = \frac{\rho}{2R}\left[\psi, v_\parallel^2 B^2\right] - \frac{\rho F_0}{2R^2}\frac{\partial (v_\parallel^2 B^2)}{\partial \phi} + \frac{1}{R}[\psi, P] - \frac{F_0}{R^2}\frac{\partial P}{\partial \phi} + \mu_0 B^2 \nabla^2 v_\parallel + S_{p_\parallel} \quad \text{(A.2)}$$

$$\rho\frac{\partial T}{\partial t} = -\rho T(\gamma - 1)\left(-2\frac{\partial u}{\partial Z} + \frac{1}{R}[v_\parallel, \psi] + \frac{F_0}{R^2}\frac{\partial v_\parallel}{\partial \phi}\right) + \rho R[T, u] - \rho v_\parallel\left(\frac{1}{R}[T, \psi] + \frac{F_0}{R^2}\frac{\partial T}{\partial \phi}\right) + \nabla\cdot\left(\kappa_\perp \nabla_\perp T + \kappa_\parallel \nabla_\parallel T\right) + S_T + S_K \quad \text{(A.3)}$$

Useful definitions are shown in table A.1.

Table A.1: Useful definitions.

μ_0	$= 4\pi\cdot 10^{-7}\mathrm{V\ s\ A^{-1}m^{-1}}$, vacuum permeability
$n_0[\mathrm{m^{-3}}]$	$=$ `central_density` $\cdot\, 10^{20}$
$\rho_0[\mathrm{kg\ m^{-3}}]$	$=$ `central_mass` $\cdot\, n_0 \cdot m_{\mathrm{proton}}$
γ	Adiabatic constant
$\parallel$	Parallel to the magnetic field
$\perp$	Perpendicular to the magnetic field
$\nabla_\parallel$	$\equiv \frac{\vec{B}}{\lvert B\rvert^2}\vec{B}\cdot\nabla$
$\nabla_\perp$	$\equiv \nabla - \nabla_\parallel$
$[A, B]$	$\equiv \widehat{\varphi}\cdot\nabla A\times\nabla B$, Poisson bracket

JOREK units and their normalisation are shown in table A.2.

Table A.2: Units used in JOREK and their SI normalisation.

SI	JOREK	Description
t_{SI} [s]	$t\sqrt{\rho_0\mu_0}$	Time
R_{SI} [m]	R	Major radius
Z_{SI} [m]	Z	Vertical coordinate
ρ_{SI} [kg m^{-3}]	$\rho\rho_0$	Mass density
n_{SI} [m^{-3}]	ρn_0	Particle number density
$\vec{v}_{\mathrm{SI}}$ [m s^{-1}]	$\vec{v}/\sqrt{\rho_0\mu_0}$	Velocity
$v_{\parallel,\mathrm{SI}}$[m s^{-1}]	$v_\parallel B_{\mathrm{SI}}/\sqrt{\rho_0\mu_0}$	Velocity
T_{SI} [K]	$T/(n_0 k_{\mathrm{B}}\mu_0)$	Temperature
T_{eV}[eV]	$T/(n_0 e\mu_0)$	Temperature (in eV)
$\vec{B}_{\mathrm{SI}}$ [T]	$\vec{B}$	Magnetic field vector
ψ_{SI} [Wb/rad]	ψ	Poloidal flux
u_{SI} [m s^{-1}]	$u/\sqrt{\rho_0\mu_0}$	Velocity stream function
D_{SI} [m^{2}s^{-1}]	$D/\sqrt{\rho_0\mu_0}$	Particle diffusivity
κ_{SI} [m^{-1}s^{-1}]	$\kappa\sqrt{\mu_0/\rho_0}$	Heat diffusivity
$S_{\rho,\mathrm{SI}}$[kg m^{-3}s^{-1}]	$S_\rho\sqrt{\rho_0/\mu_0}$	Particle source
$S_{T,\mathrm{SI}}$[W m^{-3}]	$S_T/\sqrt{\mu_0^3\rho_0}$	Heat source
F_{SI} [T M]	$F \equiv RB_\varphi$	Poloidal current stream function
E_{SI} [J]	$E/\left(\frac{2}{3}\mu_0 n_0\right)$	Energy
P_{SI} [W]	$P/\left(\frac{2}{3}\mu_0\sqrt{\mu_0\rho_0}\right)$	Power

A.2 NORMALIZATION

JOREK has a set of normalizations. The density, energy and parallel momentum contributions of the particle code must be normalized in a similar fashion to be able to be inserted in the JOREK equations. In this section the SI variants of the variables are denoted with the subscript SI, and the JOREK variables are denoted without subscript. The normalizations of density can be found directly:

$$n_{SI} = \rho n_0 \rightarrow \rho = \frac{n_{SI}}{n_0}. \tag{A.4}$$

Here n_0 is defined as the central density multiplied by a factor of 10^{20}. So ρ is adimensional.

The temperature is normalized as such:

$$T_{SI} = \frac{T}{k_{\mathrm{B}}\mu_0 n_0} \rightarrow T = T_{SI} k_{\mathrm{B}}\mu_0 n_0. \tag{A.5}$$

Where k_{B} is the Boltzmann constant and μ_0 is the vacuum permeability.

Energy is normalized as such:

$$T = K_{SI}\mu_0 n_0. \tag{A.6}$$

Where T has units $\frac{\mathrm{J\,T}}{\mathrm{A\,m^2}} = \mathrm{T^2}$.

For the parallel momentum, the velocity normalisation is needed, which can be found to be:

$$v_{\parallel,SI} = v_{\parallel}\frac{B_{SI}}{\sqrt{\mu_0\rho_0}} \rightarrow v_{\parallel} = v_{\parallel,SI}\frac{\sqrt{\rho_0\mu_0}}{B_{SI}} \tag{A.7}$$

Where B_{SI} is the magnetic field strength and $\rho_0 = \texttt{central\_mass} \cdot n_0 \cdot m_{proton}$ with $m_{proton} = 1.673 \times 10^{-27}\,\mathrm{kg}$. This quantity is adimensional.

The normalization of mass $m_{SI} = m_0 m$ can be determined with n_0 and ρ_0:

$$m_0 = \frac{\rho_0}{n_0} \tag{A.8}$$

Thus, the normalized parallel momentum is given by:

$$p_{\parallel,SI} = m_{SI}v_{\parallel,SI} = mv_{\parallel}\sqrt{\frac{\mu_0}{\rho_0}}\frac{n_0}{B_{SI}}. \tag{A.9}$$

Note that for $p_{\parallel,SI}$ to be incorporated in the JOREK equations, it has to divided by the mass of a main species atom: m_{main}. This is because JOREK works with parallel velocity.

Time is given by:

$$t_{SI} = t\sqrt{\rho_0\mu_0} \rightarrow t = \frac{t_{SI}}{\sqrt{\rho_0\mu_0}}, \tag{A.10}$$

Where t has units of $\left[\frac{\mathrm{m}}{\mathrm{T}}\right]$.